Delft University of Technology

Master Thesis Report

Full Vehicle Model of a formula student car

Full-car vehicle dynamics model incorporating a tyre model which includes the effects of temperature on it's performance.

Authors:
Diwakar Harsh, 4624009

Instructors:
Dr. Barys Shyrokau

August 20, 2018

Department of Cognitive Robotics
TU Delft

ACKNOWLEDGEMENTS

This thesis marks the end of my studies at TU Delft. The past year has been a very challenging as well as rewarding experience for me and wouldn't have been possible without the help and guidance from a lot of people.

First and foremost, I am grateful to Dr. Barys Shyrokau for giving me the opportunity to work on this project and for all his critical feedback during our meetings. I would like to thank him for his help throughout the duration of this thesis and for always being approachable. I would also like to thank Dr. A.L. Schwab and Dr. Riender Happee for taking time out and agreeing to be a part of my thesis committee.

I would also like to thank Formula Student Team Delft to allow me to work with the data and design of the previous year's car. Also, I want to extend my sincere gratitude to Apollo Vredestein B.V. who is the tyre sponsor for the team. A special thanks to my team members Tommaso, Niels, Oscar, Petar, Daniel and Simon to name a few for their unconditional support and enthusiasm that always kept me going. Not to forget the coffee breaks, discussions and all the small talks we had.

My time in Delft wouldn't have been the same if it were not for Sabya, Sagar, Manni, Ankit, Ajinkya, Sparsh, Rakshit, Varun and Nihar. I cherished the evenings we spent together. Also, cheers to my roommates Troppo, Alex, Trippy, Berci, Leesta, Sofa, Omar, Gio, Silvio and Katha with whom I could relax and enjoy my time when I was not working. I want to make a special mention to Francesco and Paul. Their support through all the lows and highs kept me going throughout the 2 years in Delft. Even after being so far away from home, spending the Christmas at Francesco's house made me feel at home.

Lastly, I would like to thank the most important people in my life: my parents and my family, for their unconditional love and support. I am eternally grateful to them for supporting me in my decision to study abroad and for their constant encouragement throughout my studies. And finally, I would like to thank God for his blessing throughout my life.

ABSTRACT

One of the important aspects in designing a formula-student vehicle is the understanding of the effects of different parameters on the vehicle's behaviour. These sensitivities help the engineers to make design decisions and reach the objectives set forth by the team. Currently, the team uses a lap simulation which uses a point mass vehicle dynamics model and thus most of the effects are not covered. This lap simulation allows to map the top-level concept of the car. However, for design of different components a full-car simulation is required that is similar to the actual vehicle.

In this Master's thesis, a full-car vehicle dynamics model is developed in the Simulink environment. The chassis model is developed using a multibody approach where the different components are modelled as rigid bodies and constrained using multibody joints. The model uses torque and steering inputs and provides outputs similar to the sensors mounted on the actual vehicle. There are two models proposed for the tyre behaviour. Firstly, the tyres are tested for steady state conditions to obtain the parameters of the basic magic formula. A thermal model for the temperature of the tyres is then proposed to obtain the tread, carcass and inflation gas temperatures. The magic formula is then extended to include the effects of temperature on the force producing capability of the tyres to achieve higher accuracy in the simulations.

A very important part of this thesis concerns the model validation. In order to ensure that the vehicle dynamics model behaves like a real car; manoeuvres performed in the dynamic events of formula student competitions were used. The skidpad and a lap of endurance event was chosen to simulate steady-state and transient behaviour of the vehicle. Moreover, the model has been tuned in an attempt to match the actual data when performing the same predefined manoeuvres. The last part of the report includes the conclusions on the model and recommendations for future work.

TABLE OF CONTENTS

NOMENCLATURE

α	Lateral slip [-]
δ	Wheel angle [rad]
$\dot{\omega}_{wheel}$	Rotational acceleration of the wheel [rad/s^2]
$\dot{r}$	Yaw acceleration [rad/s^2]
$\dot{u}$	Longitudinal acceleration [m/s^2]
$\dot{v}$	Lateral acceleration [m/s^2]
κ	Longitudinal slip [-]
μ	Friction coefficient between tyre and road [-]
ω	Wheel rotational velocity [rad/s]
ρ_{air}	Air density [kg/m^3]
A	Frontal area [m^2]
a_x	Longitudinal acceleration [m/s^2]
a_y	Lateral acceleration [m/s^2]
C_d	Drag coefficient [-]
C_l	Lift coefficient [-]
C_r	Rolling resistance coefficient [-]
C_x	Longitudinal tyre stiffness [N/-]
C_y	Lateral tyre stiffness [N/-]
CAD	Computer-Aided Design
CFD	Computational Fluid Dynamics
DAQ	Data Acquisition System
F_{drag}	Drag force [N]
F_{roll}	Rolling resistance force [N]
F_x	Longitudinal force [N]

F_y	Lateral force on the tyre [N]
F_z	Normal force on the tyre [N]
g	Gravitational acceleration [m/s^2]
h_{CoG}	Length from CoG to the ground [m]
I_{wheel}	Moment of inertia of the wheel [kgm^2]
I_z	Moment of inertia around the z-axis [kgm^2]
l_f	Length from CoG to front axle [m]
l_r	Length from CoG to rear axle [m]
m	Mass of the vehicle including driver [kg]
M_z	Moment around z-axis of the CoG of the vehicle [Nm]
r	Yaw velocity [rad/s]
r_{wheel}	Effective radius of the tyre [m]
T	Torque input on the wheel [Nm]
tw	Track width [m]
u	Longitudinal velocity [m/s]
v	Lateral velocity [m/s]
V_x	Longitudinal velocity [m/s]
wb	Wheel base [m]
h	Width of the tyre
R	Outer Radius of the Tyre and Wheel Assembly
r	Inner radius of the Tyre and Wheel Assembly

LIST OF FIGURES

LIST OF TABLES

CHAPTER 1

INTRODUCTION

1.1 Formula Student Competition

The event began as Formula SAE in the United States in 1980, and has since grown to involve over four hundred universities, with official events being held in 10 countries around the globe, and many more competitive gatherings at other locations throughout the season.

Formula Student is a competition where students build a single seat formula race-car with which they can compete against teams from all over the world [2]. The competition is not won solely by the team with the fastest car, but rather by the team with the best overall package of construction, performance, and financial and sales planning. The project aims to encourage students to be innovative, learn new skills and showcase their talents. This also presents the engineers with the chance to put theory into practice in a dynamic and competitive environment.

Formula Student Team Delft [3] has been participating in the competitions since 2001, earlier in the combustion class and since 2011 in the electric class. The team competes in a number of static and dynamic events with its electric race-car at the competition. Static events include technical inspection, cost, presentation and engineering design. The dynamic events include acceleration, skid-pad, autocross and endurance. With an aim to improve the performance of the car, the team collaborated with Apollo Vredestein B.V. in 2014 to make it's own custom tyres. Figure 1.1 showcases the 2017 car from FS Team Delft equipped with these custom tyres.

In order to get the maximum performance out of the car, the team develops a lot of vehicle dynamic tools to predict the vehicle behaviour. This was however done using estimated friction coefficient and without considering thermal effects on the tyre performance. The current lap simulation which is a point mass simulation allows for developing the top-level concept of the new car. It is able to quantify top level parameters of the car like center of gravity height, lift coefficient etc.

1.2 Objective

The main objective of the thesis is to provide a vehicle dynamic tool that allows to understand the effects of different parameters on the performance of the vehicle both qualitatively and quantitatively. An example would be the effect of spring stiffness on

Figure 1.1: DUT17 car at the Formula Student Germany competition

the average friction or lap-time of the car. The tool can also be used for optimizing the parameters such as roll-centre height, CoP location etc. and their effects on the handling of the car. In order to do so, a reliable simulation model of the car needs to be developed.

A full-car model needs to be developed to successfully replicate the behaviour of the actual car. This requires to develop a chassis model that could provide with relatively higher degrees of freedom than a bicycle or planar model. Another important requirement would be to model the custom tyres accurately. In order to do so, first the tyres would have to be tested and thus a measurement program needs to be formulated.

For an accurate model of forces and moments of the tyres and understanding of the tyres, a physical or empirical model of the tyres needs to be chosen. From literature, it was found that the temperature of the tyre has a large effect on the force producing capability of the tyre. Thus, a thermal model will also have to be developed which would be coupled to the tyre model to realize the change in performance.

1.3 Outline

Before starting the thesis work, a literature survey was conducted to find out the possible modelling techniques. This report highlights some of the literature again in the respective chapters which were used to develop the model.

The report begins with a description of the chassis model for the simulation. A multi-body modelling approach was used within the Simulink environment using the simscape multibody toolbox. This is described in chapter 2.

In order to model the tyres, tests were conducted on the Apollo and Hoosier tyres for steady state conditions using outdoor test facilities at Dynamic Test Center AG located in Vaufellin, Switzerland. The measurement program along with the results and post-processing is provided in chapter 3.

A thermal model for the tyre temperatures is proposed in chapter 4. The chapter discusses some of the models from literature which were used as benchmark for the new model. Modifications have been then proposed for the models and the performance of the thermal models was compared with the measurement data.

The magic formula from Pacejka is used in the simulation due to it's accuracy and low computation effort. However, the magic formula does not incorporate the effects of temperature on tyre behaviour. Thus, an extended magic formula is proposed which takes into account the temperature effects. The basic and extended magic formula is described in chapter 5

The complete tyre and vehicle model is then described in chapter 6. The model structure along with the inputs and outputs are described. Finally, the model is validated by comparison with sensor data from the car for steady state and transient manoeuvres.

The report concludes with a summary and conclusions of the master thesis described in chapter 7. Recommendations for future work are also formulated.

CHAPTER 2

CHASSIS MODEL

2.1 Introduction

The chassis model is one of the important blocks of the vehicle model. It is the component which defines the motion of the vehicle by gathering all the information and states of different sub-systems of the vehicle dynamic model.

Multi-body systems analysis is applicable to mechanical systems that may be built from an assembly of rigid bodies. The relative motion between the bodies is constrained using constraint elements, or joints, which represent real mechanical connectors such as universal joints. It is also possible to model flexible connectors such as rubber bushings. Within the automotive industry the main use is involved with the design and analysis of vehicle suspension systems and the prediction of the ride and handling performance of the total vehicle.

For a full vehicle model intended for handling simulations, a large amount of data might be required to solve equation based-models. Multi-body systems analysis, however, utilizes a modelling approach where mechanical components are generally treated as rigid bodies [4].

This chapter thus, discusses the assumptions and implementation of a multibody chassis model that was used for the full-vehicle model of the DUT17 car.

2.2 Assumptions

In order to model the chassis system of the car, several assumptions were made to simplify without losing accuracy in the simulations. The assumptions made for the multi-body model are described below:

- All joints and bodies except the tyres and springs are considered rigid. Compliance under load application is not considered since the suspension and chassis are designed to be stiff. Friction in bearings and joints is also not considered. However, there is some damping provided in the revolute joints between the suspension and the wheels to model the transmission friction.
- The position of the center of gravity, mass and inertia of the chassis including the driver are taken from the combination of the CAD model and actual measurements

on the final car. The suspension linkages are imported from the CAD assemblies providing the exact geometry as on the actual car.

- Aerodynamic forces are assumed to be acting on a constant center of pressure which was calculated from CFD simulations in steady state conditions. In reality, the center of pressure changes depending on the velocity, roll, pitch etc. of the car.
- The suspension springs and dampers are actuated using a pull/push rod as designed on the car. They are also linear in the range of the operation.

2.3 Model of the Formula Student Car

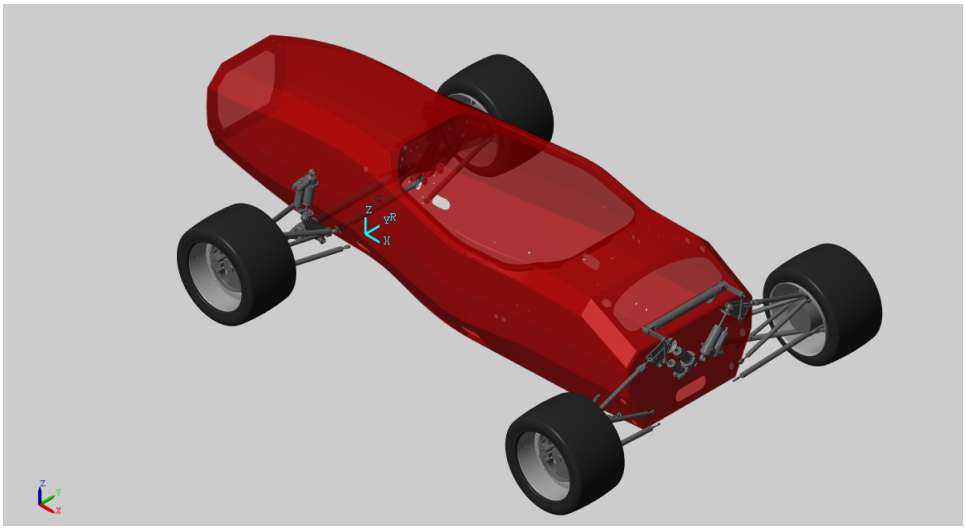

Figure 2.1: Visualization of the chassis model along with the co-ordinate system

The model is developed in the Simulink environment of Matlab & Simulink software. The multibody modelling is done using the simscape multibody toolbox. The model uses the coordinate system similar to the CAD design where gravity acts in the negative z-direction. The origin lies on the ground at the center of the vehicle below the front vehicle. Positive x-direction is towards the rear of the car and positive y-direction is towards the right of the car. An overview of the coordinate system is shown in figure 2.1.

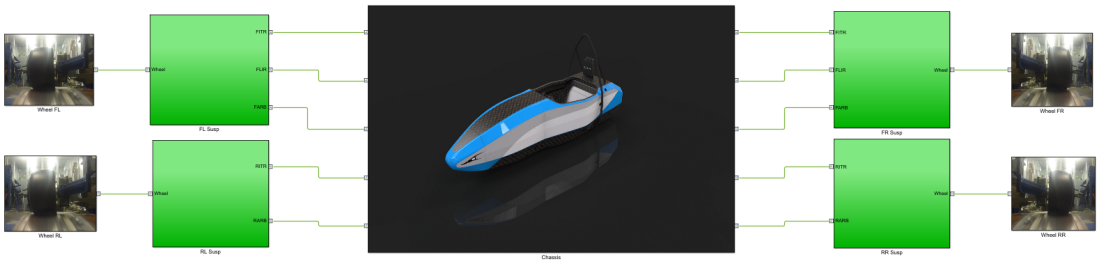

Figure 2.2: Overview of the complete model

The model consists of four suspension subsystems connected to the chassis body. Each

subsystem contains suspension linkages imported from CAD. The tyre is connected to the suspension system using revolute joints from the upright center. A steering system is also provided which is connected to the front suspension and the chassis body through different joints. The visualization of the model is shown in figure 2.1 and the overview of the complete system is provided in figure 2.2.

2.3.1 Chassis System

The chassis system is the centre block which is connected to all other systems as shown in figure 2.2. It consists of the world frame, the chassis body and sensors and actuators for the application of the aerodynamic forces and measuring roll & pitch angles. The chassis body can move freely in the world and thus is connected to the world frame using a 6-DoF joint. The overview of the chassis system is shown in figure 2.3. As mentioned in the assumptions, the aerodynamic forces are applied on a constant center of pressure value.

The rockers are mounted on the chassis using revolute joints. These rockers transform the suspension travel to compression or rebound of the spring damper system. The casing of the damper is also connected to the chassis using revolute joints to transfer the load from the suspension to the chassis. As mentioned earlier, the steering system is also connected to the chassis. This is done using a translational joint which allows for the push/pull action on the tie-rods. The last connection to the chassis is with the anti-roll bars. The brackets for the anti roll bars are connected to the chassis using a weld joint to provide support for the ARB.

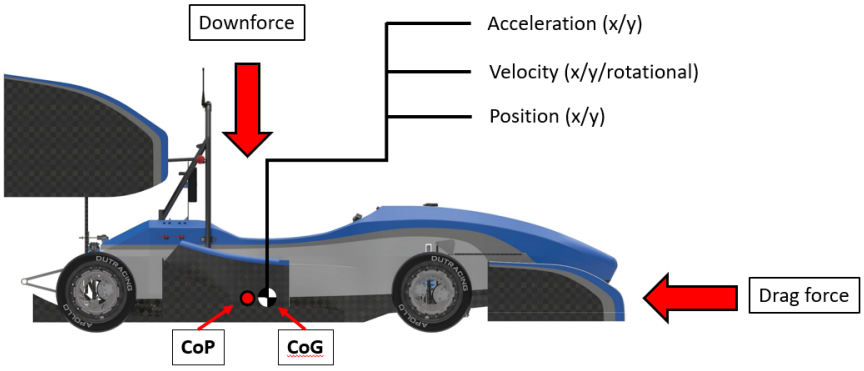

Figure 2.3: Representation of the Chassis System block

The parameters used for the chassis system are now presented in table 2.1. To be able to make an accurate model, parameters such as mass, inertia etc. needs be as close as possible to the actual vehicle. Combined use of CAD software such as Catia and actual weights from scales were used for measuring the different parameters.

Parameter	Value	Units	Measured/Estimated
Wheelbase	1.53	m	Measured
Track Width	1.2	m	Measured
CoG longitudinal distribution	50	%	Measured
CoG lateral distribution	50	%	Measured
CoG Height	0.3	m	Estimated

CoP longitudinal distribution	54	%	Estimated
Lift Coefficient	3.5	-	Estimated
Drag Coefficient	1.53	-	Estimated
Mass of Driver	70	kg	Measured
Sprung Mass	180	kg	Estimated
Yaw Inertia	137.5	kgm^2	Estimated
Roll Inertia	50	kgm^2	Estimated
Pitch Inertia	87.5	kgm^2	Estimated

Table 2.1: Parameters for Chassis System

As it was not possible to physically test for inertia the different components, it was decided to use the CAD software to evaluate the inertia. Given the number of components in the whole car assembly, it was not possible to input the material properties of all the components and hence the inertia of the car was evaluated using only the heaviest parts of it. The results found out are shown in table 2.1.

2.3.2 Suspension System

As mentioned earlier, each suspension system (the green blocks in figure 2.2) contains linkages imported from CAD. The linkages are coupled to the upright using spherical joints. An overview of the suspension is system is shown in figure 2.4. The wishbones are connected to the chassis body on the car using rodends which are spherical joints. However, in the model one of the spherical joint is replaced with a telescoping joint which also has one translational degree of freedom apart from the 3 rotational DoF. This translation degree of freedom is in the x-direction, because in this direction both joints of an A-arm with the chassis restrict the same movement which would give an over-determined system.

The front suspension consists of a pull-rod mechanism with push-rod mechanism at the rear to actuate the dampers. The pull/push rods are connected to the rocker which also provides mounting points for the damper and ARB. The pull/push-rods and the tie rods in reality are also connected using the rodends with 3 DoF. However, the rotation is usually restricted around it's own axis. In order to prevent the rotation of these linkages around their own axis, a universal joint is used on one end instead of a spherical joint.

The damper in the actual car has spherical bearings at the mounting points to account for manufacturing tolerances. However, in the model it is mounted to the rocker using revolute joints since, the actuation takes place in a single plane. The damper consists of 2 bodies, the casing and the piston rod connected through a cylindrical joint. A spring/damper force is also applied between the two bodies. The damping and spring force action depends on the relative position and velocity of these two bodies.
In order to add the mass and inertia of the electric motor which is mounted on the upright in the car, a solid cylinder is used with the same mass as the motor. This cylinder is coupled with the upright using a weld joint.

The values of the suspension parameters were based on the design variables of the DUT17 car and are presented in table 2.2. The roll center height and the anti pitch was

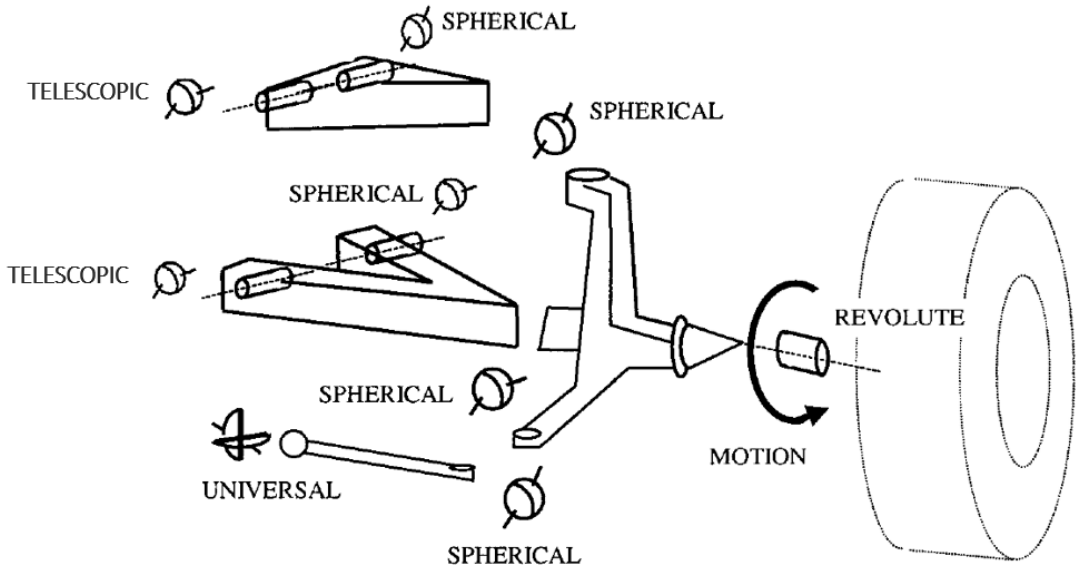

Figure 2.4: Overview of the Suspension System block

Parameter	Value	Units	Measured/Estimated
Spring Stiffness	4000	N/m	Measured
Damping Coefficient	2000	Ns/m	Measured
Anti-Pitch	30	%	Estimated
Roll center front	0.0492	m	Estimated
Roll center rear	0.0841	m	Estimated

Table 2.2: Suspension Parameters of the DUT17 car

achieved by using the suspension links from CAD and using the correct mounting points. A simple illustration is showed in figure 2.5 that explains the calculation of roll center heights. The pitch center was found in a similar manner in the side view of the car. The anti pitch then depends on the height of the pitch center with respect to the centre of gravity height.

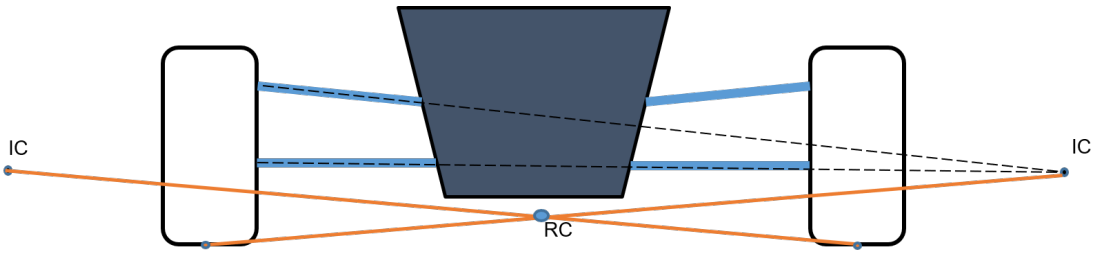

Figure 2.5: Illustration to show roll centre height evaluation

2.3.3 Steering System and Anti Roll Bars

The steering system is included in the chassis block in the overview of the complete model. It consists of a rigid body for the z rack and is connected to the front tie-rods. It is also

connected to the chassis body using a translational joint in the y-direction. This joint is actuated using the data from the actual car to provide steering input in the simulation. The representation of the steering system is shown in figure 2.6a.

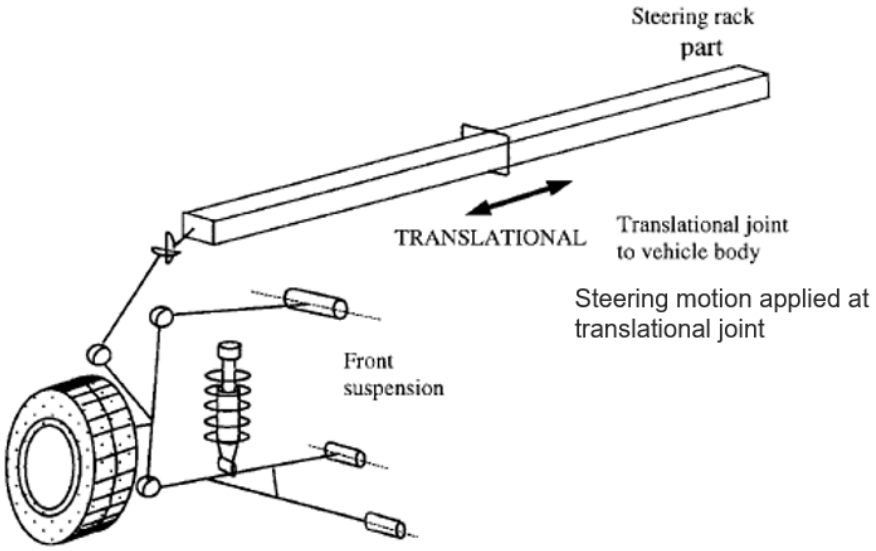

(a) Steering System block

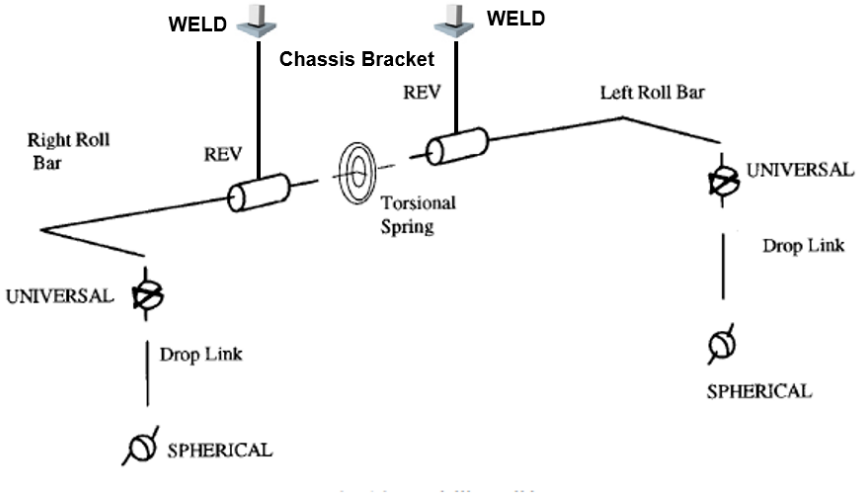

(b) ARB system block

Figure 2.6: Representation of the ARB and Steering Model

There are anti-roll bars modelled on both the axles. Again the rigid bodies are imported from CAD. However, since a torsion bar cannot be modelled, the model uses a torsion spring in between the ARB rod and the droplink from the rockers. The droplink and the ARB lever is connected to the rod using revolute joints. The roll bar is held in place by using support brackets that are connected to the chassis. The representation of the anti-roll bar system is shown in figure 2.6b.

The parameters for the steering and ARB system is shown in table 2.3. In the actual car, the anti-roll bar stiffness is slightly different since the chassis is not completely rigid and the stiffness was adjusted based on driver feedback. However, in the model the

Parameter	Value	Units	Measured/Estimated
Steering Ratio	0.17	mm/deg	Measured
Front Anti-Roll Bar stiffness	125	Nm/deg	Measured
Rear Anti-Roll Bar stiffness	75	Nm/deg	Measured

Table 2.3: Steering and ARB parameters

chassis is rigid and the stiffness was adjusted to get similar under/over-steer behaviour.

2.3.4 Tyre and Wheel Parameters

Th tyre force model will be discussed later in the report. However, the mass and inertia parameters for the tyre and wheel assembly are included in this chapter. The mass and dimension properties were easily measured, however, the inertia paramters were estimated. The measurable properties of the assembly are described in table 2.4.

Parameter	Value	Units	Measured/Estimated
Mass	4.1	kg	Measured
R (outer radius)	0.17	m	Measured
r (rim radius)	0.127	m	Measured
h (width of the tyre)	0.225	m	Measured
Aspect Ratio [5]	0.249	-	Estimated
Tyre inflation pressure	0.6	bar	Measured

Table 2.4: Parameters for the Tyres and Wheel

A fundamental parameter of the tyre is its inertia. An accurate value is key to correctly model the acceleration and deceleration of the wheels. Unfortunately there is no simple way to measure it and the CAD model of the tyre was not reliable enough to yield to a correct estimate. This parameter was estimated by simplifying the tyre to a uniform hollow cylinder as depicted in figure 2.7.

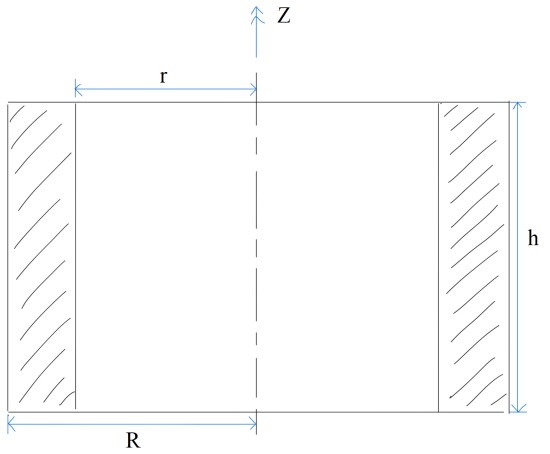

Figure 2.7: Simplification of the tyre and wheel assembly for inertia estimation

The inertia's for the tyre and wheel assembly along the three principal axis were computed

using the following formulas.

$$I_z = \frac{m}{2}\left(R^2 + r^2\right) = 0.09 \text{ kgm}^2 \tag{2.1}$$

$$I_x = I_y = \frac{m}{12}\left(3\left(R^2 + r^2\right) + h^2\right) = 0.06 \text{ kgm}^2 \tag{2.2}$$

2.4 Summary

This chapter describes the base vehicle model that will be used for the simulations. The assumptions and the implementation of the chassis model were also discussed. The next step was to use a tyre model that could map the behaviour of the custom tyres of the team. The next chapters describes the testing of these tyres and the development of a tyre model (thermal and mechanical) that would be implemented to improve the accuracy of the complete simulation.

CHAPTER 3

TYRE TESTING

3.1 Introduction

A good prediction of the tyre forces and moments is necessary to assess the vehicle handling and tune the vehicle's suspension layout for optimum performance. The use of custom built tyre at Formula Student Team Delft meant they had to be tested to understand their behaviour and performance. The testing of the tyres was also important to evaluate the gains and understand the difference in behaviour with market available formula student tyres.
The measurement of the tyre performance was performed at Dynamic Test Center AG located in Vaufellin, Switzerland. A brief overview of the test program can be seen in table 3.1. The test program consisted of a number of slip angle, α and wheel slip $\kappa-$sweeps for different normal loads.

Measurement	**Tyre**	$\boldsymbol{\alpha}[^\circ]$	$\boldsymbol{\kappa}[-]$	$\boldsymbol{F_z}$ **[N]**
Pure Cornering	Apollo Single Compound	α sweep	0	600 / 1000
	Apollo Double Compound	α sweep	0	600 / 1000
	Hoosier	α sweep	0	600 / 1000
Pure Braking	Apollo Single Compound	0	κ sweep	600 / 1000
	Apollo Double Compound	0	κ sweep	600 / 1000
	Hoosier	0	κ sweep	600 / 1000
Pure Acceleration	Apollo Single Compound	0	κ sweep	600 / 1000
	Apollo Double Compound	0	κ sweep	600 / 1000
	Hoosier	0	κ sweep	600 / 1000

Table 3.1: Tyre Test Program

In this chapter, the description of the test setup is provided along with the measurement data and it's analysis. The first section describes the test equipment and it's calibration. This is followed by results of the measurements and comparisons between the different tyres. The next section describes the post-processing performed on the raw data followed by parameter estimation to fit the measurements to the Magic Formula as used in Delft Tyre software provided by TNO Automotive [6].

3.2 DTC Morelab

This section describes the various elements of the test truck (DTC MoreLab) used for testing the tyres. The section also describes the calibration procedure and a brief overview of the controller for different sweeps.

Figure 3.1: Tyre Testing with DTC MoreLab

3.2.1 MoreLab Capabilities

A Kistler measurement hub [7] was used to measure the forces and moments from the tyre. The hub is built in two pieces and consists of piezoelectric sensors in the middle of the casing. The sensors reads the forces and moments in all 3 dimensions by measuring pressure distribution across the hub. It can be used for a wide range of temperatures.

The Normal load during the test run was controlled by the use of hydraulic suspension. Before the test the hydraulic pressure was adjusted to achieve the desired normal load on the tyre. The movement of the suspension allowed to account for the irregularities in the test track. The suspension also allowed change in the camber angle by the use of shim plates on the upper A-arm of the double wishbone suspension geometry.

For acceleration and braking measurements, the wheel was driven using a motor which was powered from the truck engine. The torque was transmitted using an axle shaft and thus could be used for both braking and acceleration measurements.

Another actuator is provided on the tie-rod that is used for generating slip angle in the tyre. All the actuators on the truck are controlled by the means of a SPS controller (PLC) which can be activated using the console inside the truck cabin.

Figure 3.2: Test Setup on the MoreLab truck

To measure the temperature of the tyres during the test, three optical temperature sensors were mounted to get the temperature profile across the tyre width. An overview of the complete test setup is shown in figure 3.2 and the console for the controller in figure 3.3.

Figure 3.3: Console inside the cabin of MoreLab

3.2.2 Calibration

The measuring hub was first calibrated with forces in the lateral and normal load direction for each tire dimension. In order to get the calibration of the forces correct, focus was laid on the angle of the application of force. Figure 3.4 provides an overview of the calibration procedure carried out for the measurement hub in the lateral direction for the Apollo tyre.
In order to calibrate the α-sweep, a grid representing the steering angle of the tyre was

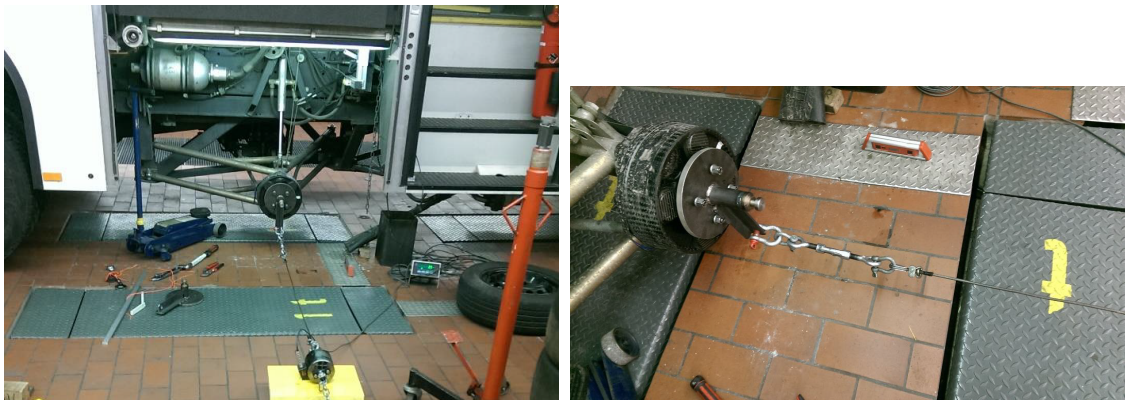

(a) Force Calibration - front view (b) Force Calibration - top view

Figure 3.4: Force Calibration for Apollo Tyres in lateral direction

arranged on the floor. A laser is mounted on the wheel hub which moves over the grid in order to compare the actual angle with the electrically controlled angle from the actuator. This measurement also allows to correct any hysteresis present in the automated sweep. The setup for the calibration is shown in figure 3.5.

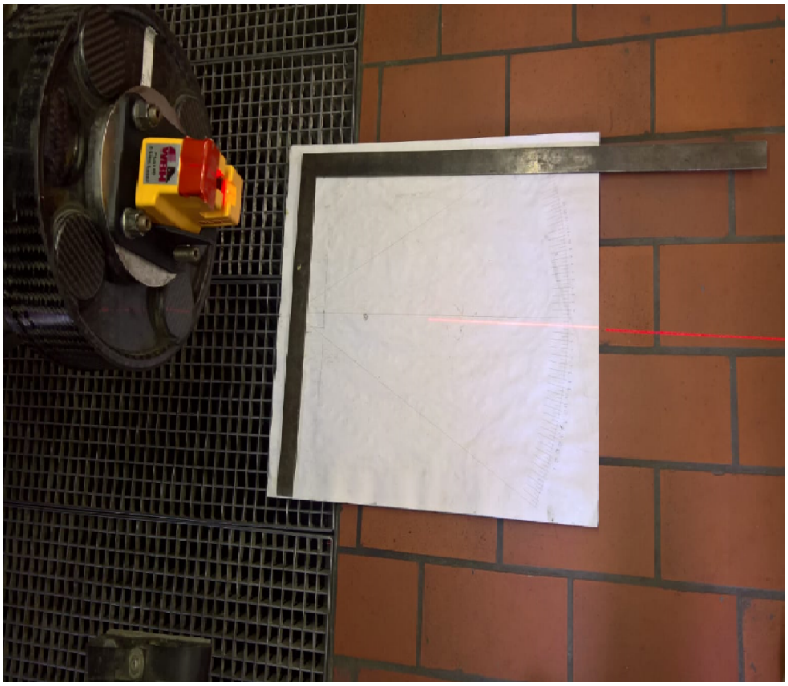

Figure 3.5: Calibration of Automated Slip angle (α) sweep

3.3 Measurements

This section describes the raw measurement results for the test program. It was made sure that the tyres reach optimum temperature before the measurements were recorded. This was done by performing the test run without recording the measurements and the

temperatures were monitored using the hardware interface at the control unit inside the truck cabin.

3.3.1 Pure Cornering

The lateral performance of the tyres was assessed by performing automated α-sweeps at a constant rotational speed of 15 deg/sec. The sweeps were performed at two different normal loads. However, due to road modulation and other irregularities, the vertical force fluctuated and thus influenced the lateral force measurement. This influence is countered by using the friction plots and then multiplying by mean vertical load to get the lateral force plots. The plots for pure cornering are as shown in figure 3.6.

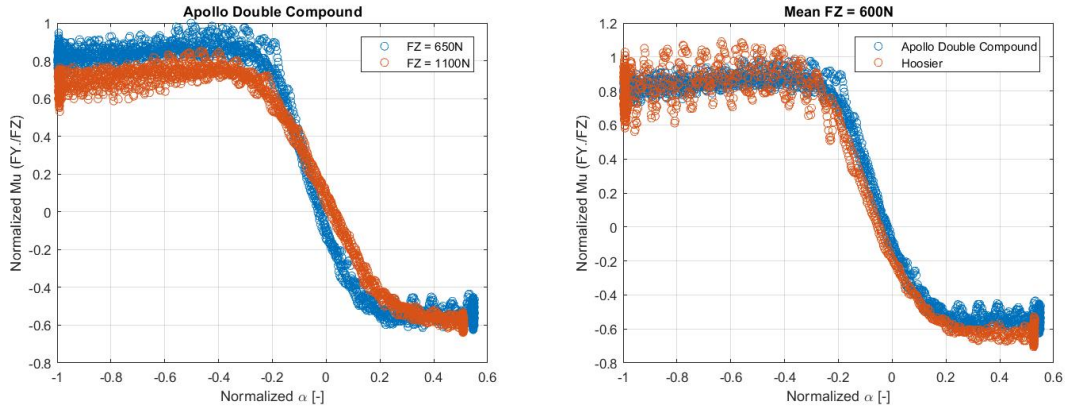

(a) Lateral Performance with Slip Angle

(b) Lateral Performance Comparison

Figure 3.6: Normalized Mu with slip angle

The figure 3.6a explains the influence of vertical load on the friction coefficient and agrees with the expected result that the friction coefficient decreases with vertical load. In figure 3.6b, the results of Hoosier and Apollo tyres are compared. It can be seen that the peak friction of the Hoosiers is higher than the Apollo but the average friction is quite similar.

3.3.1.1 Cornering Stiffness

The cornering stiffness of the tyre is defined as the linear relationship between the lateral force and the slip angle for small slip angle. The cornering stiffness is extracted from the measurements at zero camber angle and is calculated as:

$$C_{F_\alpha} = \frac{\partial F_y}{\partial \alpha} \tag{3.1}$$

The results of the cornering stiffness at different normal loads are shown in figure 3.7. The cornering stiffness of the Apollo tyres is higher than the Hoosier's at lower normal loads. This can be attributed to the construction of the tyres. The Apollo tyres have a larger width and a smaller sidewall as compared to the Hoosiers. Thus, at higher loads the Hoosier tyres have enough sidewall to provide extra stiffness as compared to the Apollo's. There is also some difference between the two Apollo tyres which is mainly due to the difference in compound properties, since, the internal structure for both the tyres is same.

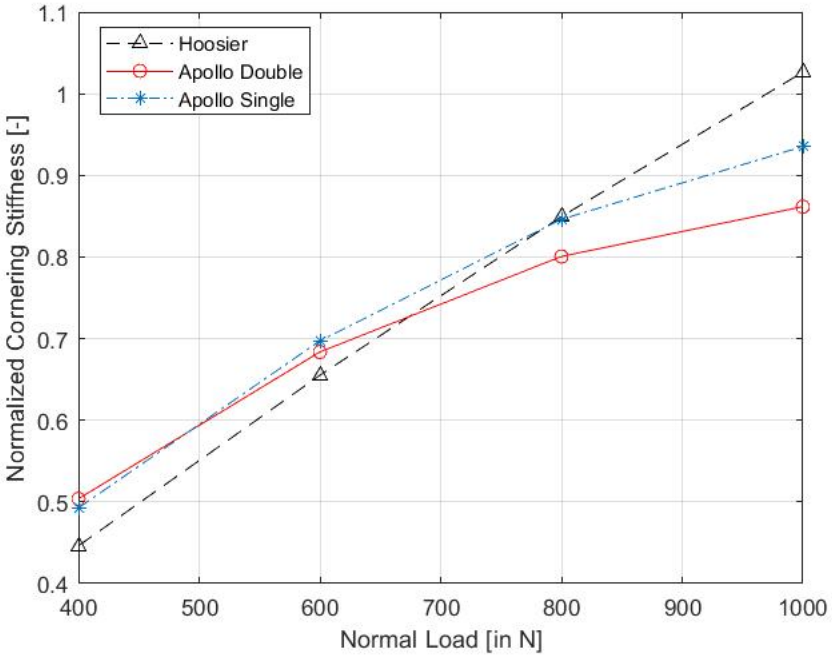

Figure 3.7: Normalized Cornering Stiffness with Normal Load

3.3.2 Pure Acceleration and Braking

For the longitudinal force measurement, the lifted wheel was first accelerated and then the normal force was applied. After the wheel was on the ground, braking torque was applied to approximately 40% slip while the forward velocity of the truck(MoreLab) was kept constant. The results are shown in figure 3.8. It can be seen in figure 3.8a that the affect of normal load on friction is much less as compared to lateral friction. Also, from figure 3.8b, the performance of Apollo tyre can be compared to Hoosier tyre. The difference in the performance was found to be around 3% which can be due to the ambient conditions and track temperature.

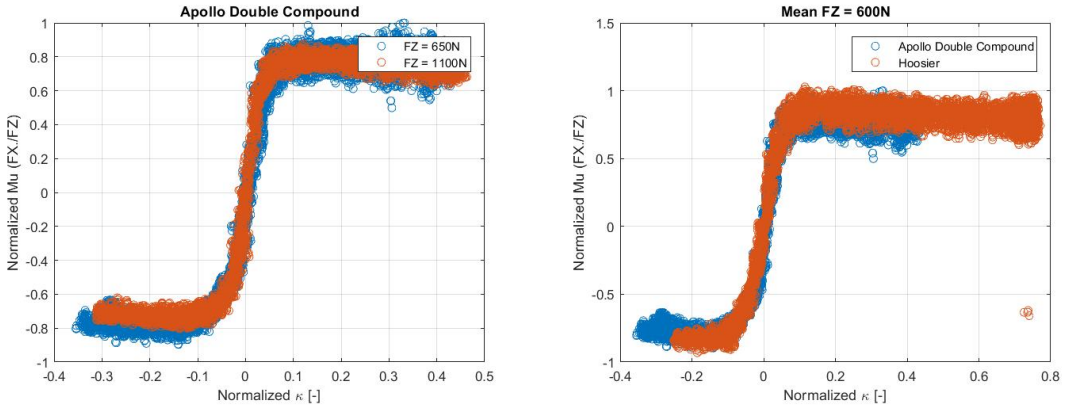

(a) Longitudinal Performance with κ (b) Longitudinal Performance Comparison

Figure 3.8: Normalized Mu with longitudinal slip

3.4 Post-Processing and Parameter Identification

Since, there are a lot of factors that affect the measurements, post-processing was required to achieve sensible results for parameter estimation. The influences are discussed in the section along with the processing tools used to correct them. The section concludes with providing a description about parameter identification for the Magic Formula.

3.4.1 Measurement Selection

For each type of run, there were a number of measurements that were recorded which led to slight differences due to operator errors or surface irregularities. As can be seen in figure 3.9, there were some measurements which had to be omitted from the final results since the behaviour was not recorded properly. This was done by the use of a GUI interface developed at DTC. The GUI loads the raw data from text files into matlab and enabled to remove or cut-off the measurements in order to choose the correct ones.

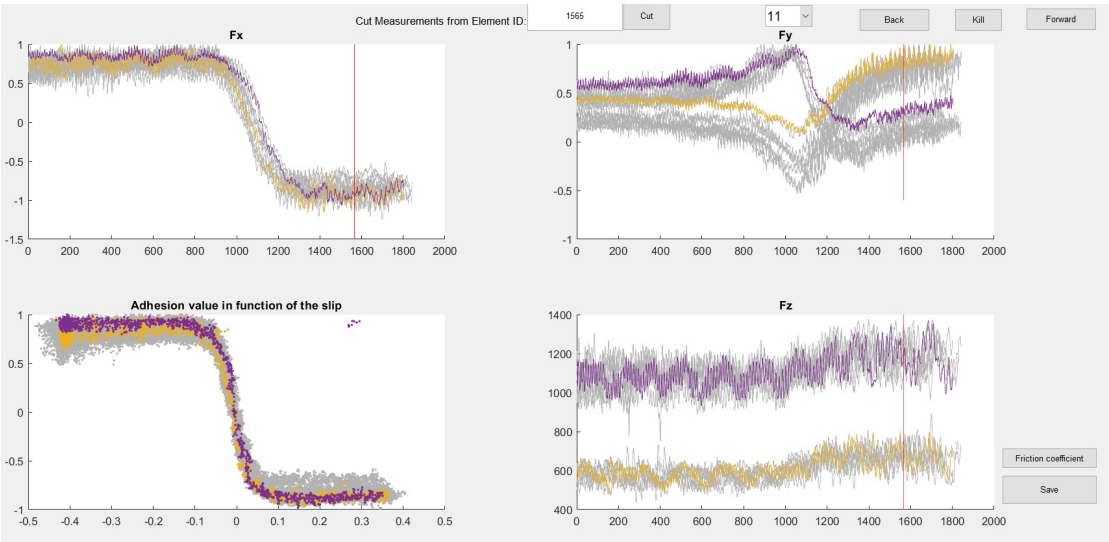

Figure 3.9: GUI interface to select measurements

3.4.2 Drift Compensation

The next step after the raw measurements were selected was to compensate for the drift within the different sensors. This was done by measuring the 'zero value'(value when no force is applied) at the beginning and the end of the measurements. This value provides the offset which is then removed from the raw measurements to compensate the drift in the sensors. An example of the drift compensation is showed in figure 3.10.

3.4.3 Temperature Effects

From literature, it is known that the temperature plays a crucial role in determining the performance of the tyre. The temperature of the tread in itself depends on large number of factors such as the normal load, ambient conditions etc. Since there was a difference in normal load during each measurement (two tyres were tested simultaneously), the temperature profile of the tread were different on the two tyres as shown in figure 3.11.

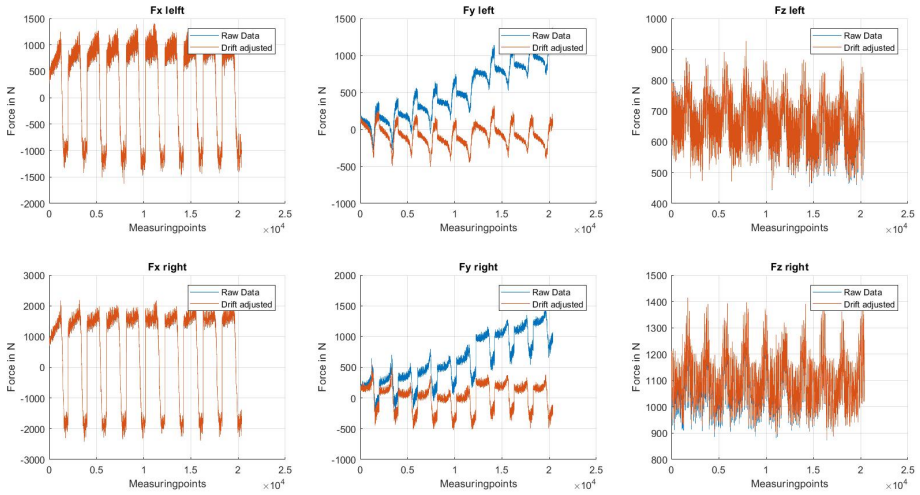

Figure 3.10: Drift compensation

Thus, it was important to choose the measurements for the two tyres such that they were in a similar temperature range.

3.4.4 Parameter Identification

Once the measurements are processed for different errors and selected according to similar temperatures, they were converted to files with a specific format. The Tyre Data Exchange Format (TYDEX) has been developed and unified by an international tyre working group to make the tyre measurement data exchange easier. The use of this format enabled the use of MF Tool software provided by TNO Automotive. The MF tool software fits the magic formula coefficients according to the test data provided from the measurements. Figure 3.12 shows an example of the fit on the measurements from Hoosier tyres. The MF Tool after the fit can also create a tire property file that can further be used for vehicle dynamic simulations based on magic formula.
As can be seen in the figure 3.12, the MF Tool also compensates for the variation in normal load and fits the curve for a nominal load. It then provides a coefficient that influences the force producing capability of the tyre based on the normal load.

3.5 Summary

This chapter described the testing process undertaken to get the measurements which will then be further used in the thermal and tyre modelling process. It also described the post-processing tools that were used to filter the measurement data and use the optimum performance of the tyres. The measurements were then fitted to the extended magic formula using MF Tool at their optimum performance and tyre property files were created that could be used in the base vehicle dynamics model.

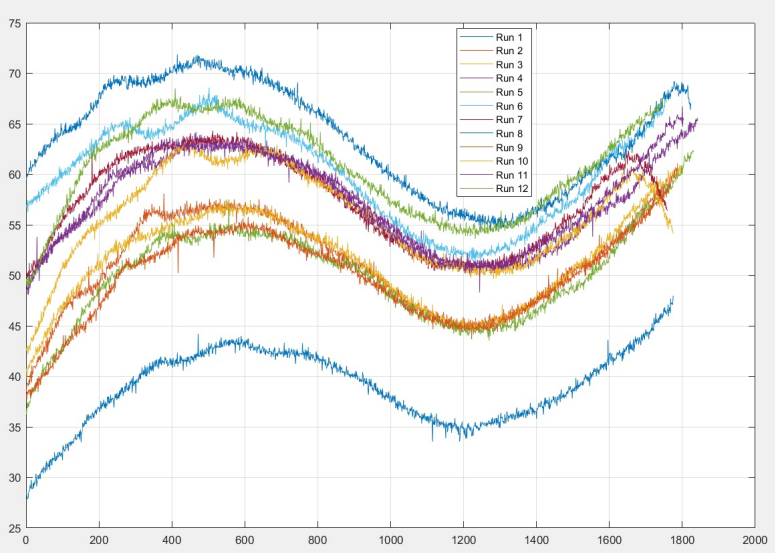

(a) Temperature Profile with Fz = 600N

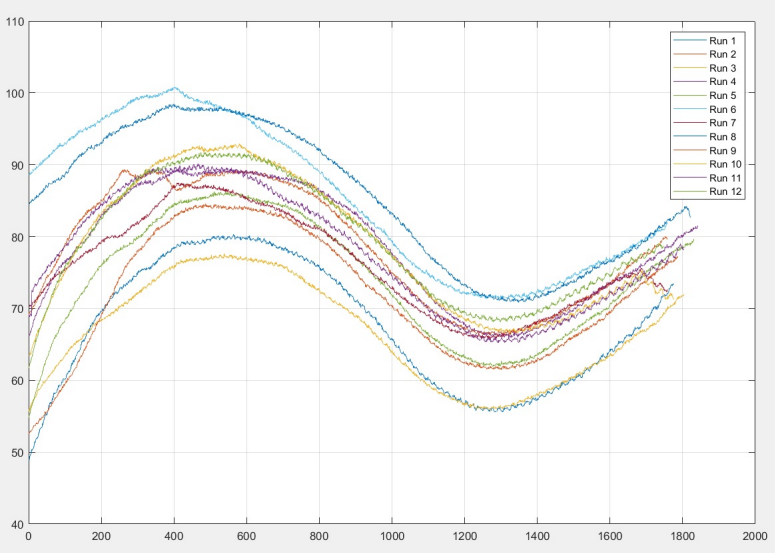

(b) Temperature Profile with Fz = 1000N

Figure 3.11: Temperature variation with different normal loads

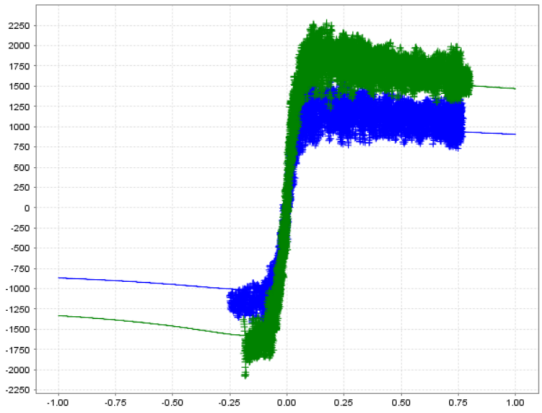

Figure 3.12: Fit for Magic Formula of measurement from Hoosier Tyre

CHAPTER 4

THERMAL MODEL FOR TYRES

4.1 Introduction

The current state of the art for tyre modelling is based on mathematical formulas that are fitted to indoor test machine measurements. These can represent the tyre characteristics for a wide variety of tyre types and sizes, but the forces and moments they describe are only representative of indoor measurement conditions that the model is based on, and the quality of the model prediction is completely linked to the measurement protocol. However, because indoor tests cannot cover all the actual driving conditions, such an approach that disregards the influence of thermal effects remains limited to a few vehicle manoeuvres. Literature mentions differences between the field tests and the steel drum:

- SAE International mentions that the lateral forces generated by the flat belt are approximately 10% higher than a steel drum can generate. [8]
- Whitcomb shows that road surface generates more lateral force than the steel drum. [9]
- Bergman says that although drum and trailer curves have similar shapes and show similar trends, there are considerable discrepancies between the absolute values of cornering stiffness obtained from trailer and drum tests. Additionally at slow steering rates the tyre stiffness is increased on a steel drum compared to using a trailer. [10]

However, the behaviour might have a big difference depending on the temperatures on which the tyres are run. Tyre temperature affects both the force-producing capability of the tyre and also the life of the tyre. The tyre carcass is an elastic device that is partly responsible for the cornering stiffness. A change in temperature will change the modulus of elasticity of the rubber (unlike steel where this is constant over a large temperature range) and affect the cornering stiffness. A comparison of tyre performance at two different operating temperatures is shown in figure 4.1.

Tyre pressure and temperature are interrelated-lower initial pressure results in more rubber distortion and higher temperature, which in turn results in higher "hot" pressure. If too cold, the tyres are very slippery; if too hot the tread rubber will 'melt'; in between is the correct temperature for operation. In addition, the tyre's temperatures change continuously as the pressure, speed and operating forces vary [11].

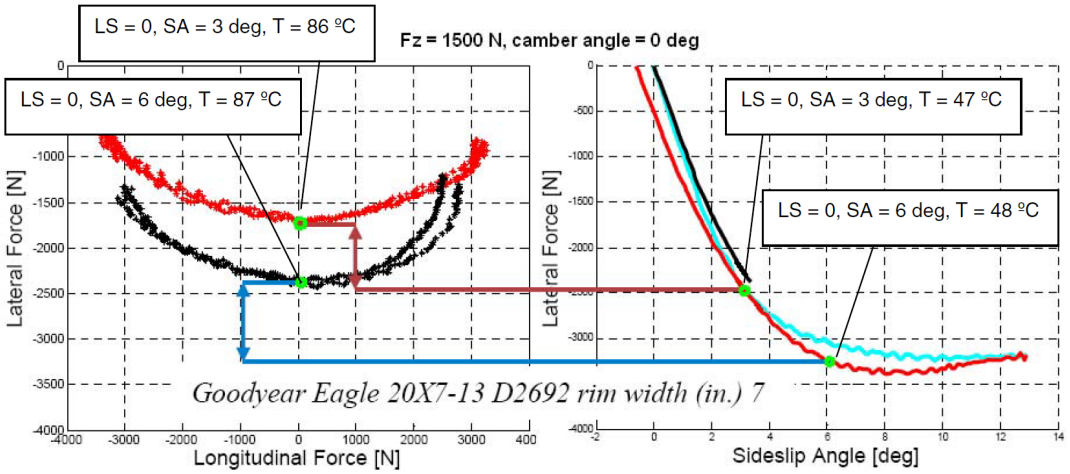

Figure 4.1: Comparison of tyre performance at two different operating temperatures T at same conditions of longitudinal and side slip angle

This chapter describes the various thermal models that are applied to existing tyre models and their performance to map the temperature obtained from measurements. A few improvements are then implemented to one of the benchmark models and the resulting improvement in accuracy is compared. For the benchmark models, the model from Aldo Sorniotti [12] and the model developed by Kelly and Sharp [13] are used given their simplicity and relatively accurate output results. The difference in the models arises from the order of differential equations, however, the basic equations are similar.

4.2 Benchmark Models

4.2.1 Model by Aldo Sorniotti

This model presents an empirical model for the estimation of tire temperature as function of the actual working conditions of the component. The estimated temperature values enter a tire brush model and provoke the variation of the performance in terms of tangential forces. The model can be empirically tuned through experimental data showing the variation of tire performance as function of temperature.

There are two thermal models that have been developed. The first one (Model 1) considers the whole tyre as an equivalent thermal capacity. The second one (Model 2) considers the tyre as a system of two thermal capacities, simulating the different temperature dynamics of the tread and the carcass of the tyre. The two models will be described in brief below.

Model 1

In this model, the tyre is modeled as an equivalent thermal capacity, $C_{eq,tyre}$, which is subjected to different power fluxes as mentioned below. The structure of this model is shown in figure 4.2.

- A power flux ($P_{rolling\_resistance}$) related to the tyre rolling resistance which are dissipations internal to the carcass of the component.

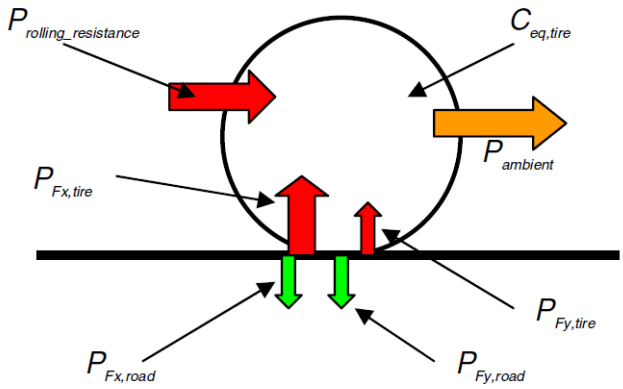

Figure 4.2: Schematic of Model 1

- A power flux related to the generation of longitudinal force because of longitudinal slip. A fraction λ of this energy is dissipated at the contact patch and enters the tyre (P_{Fx_tyre}) while the remaining part heats the road (P_{Fx_road}).
- A power flux related to the generation of lateral force because of lateral slip. A fraction λ of this energy is dissipated at the contact patch and enters the tyre (P_{Fy_tyre}) while the remaining part heats the road (P_{Fy_road}).
- A power flux ($P_{ambient}$) which is related to the cooling flux due to the temperature difference between tyre tread and ambient.

Applying the first principle of thermodynamics lead to the following equation :

$$C_{eq\_tyre}\frac{dT}{dt} = P_{rolling\_resistance} + P_{Fx\_tyre} + P_{Fy\_tyre} + P_{ambient} \tag{4.1}$$

where,

$$P_{Fx\_tyre} = \lambda\left|(F_x v_{sx})\right| \tag{4.2}$$
$$P_{Fy\_tyre} = \lambda\left|(F_y v_{sy})\right| \tag{4.3}$$
$$P_{ambient} = h(T_{ambient} - T) \tag{4.4}$$

This model is, hence characterized by a first order differential equation. The steady state temperature of the tyre(for constant power flux) is given by:

$$T = T_{ambient} + \frac{P_{rolling\_resistance} + P_{Fx\_tyre} + P_{Fy\_tyre}}{h} \tag{4.5}$$

The drawback of this kind of tyre model is that it cannot be adopted in order to achieve a good estimate of the temperature of the surface of the tread, as it is characterized by significant oscillations as functions of the time histories of longitudinal slip and sideslip angle. Model 2 takes into account the different temperature dynamics of the carcass (characterized by low frequency dynamics) and the tread of the component (characterized by much higher frequency dynamics).

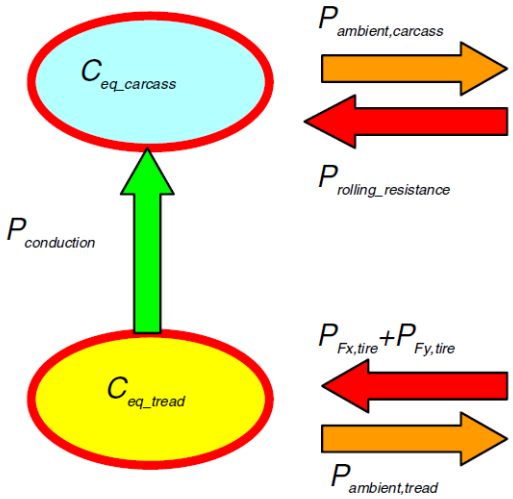

Figure 4.3: Schematic of Model 2

Model 2

In this model, there are two distinct thermal capacities for the tread and the carcass of the tyre. The structure of this model is shown in figure 4.3. The thermal capacity which represents the tread is subjected to the heat flux related to the longitudinal and lateral forces between the tire and the pavement. A second thermal flux is due to the ambient. A third conductive flux is exchanged between the two capacities. The capacity which represents the carcass receives the power flux related to the rolling resistance and exchanges heat with the external ambient.

The model is then characterized by the following equations:

$$C_{eq\_carcass}\frac{dT_{carcass}}{dt} = P_{rolling\_resistance} + P_{cond} + P_{ambient,carcass} \tag{4.6}$$

$$C_{eq\_tread}\frac{dT_{tread}}{dt} = P_{Fx\_tyre} + P_{Fy\_tyre} - P_{cond} + P_{ambient,tread} \tag{4.7}$$

where,

$$P_{ambient,carcass} = h_{carcass}(T_{ambient} - T_{carcass}) \tag{4.8}$$

$$P_{ambient,tread} = h_{tread}(T_{ambient} - T_{tread}) \tag{4.9}$$

$$P_{cond} = h_{conduction}(T_{tread} - T_{carcass}) \tag{4.10}$$

The conduction to the road in this model is not considered which is added to the model to improve the performance. The steady-state temperatures for model 2 are different for the tread and the carcass. Since, Model 2 has higher order of differential equation, it was used in the benchmark model. The higher order of differential captures more dynamics related to heat transfer and thus produces better results.

4.2.2 Model from Kelly and Sharp

D.P. Kelly and R.S. Sharp [13] states that in motor racing, the tyre friction depends largely on the temperature of the tread rubber. The temperature affects both the tyre

stiffness and the contact patch friction, although the effect on the friction is higher. The visco-elastic properties of the rubber depend on temperature. The maximum performance on the race track, which is dependent on the visco-elastic properties of rubber, is only available in a small temperature range.

Friction Model

The basic principal of the tyre model is based on the brush-model approach. The adhesion part is described using the bristle stiffness c_p.
For the adhesion part:

$$c_p = \frac{w_{cp} G_{tread}}{h_{tread}} \tag{4.11}$$

with shear modulus given by:

$$G_{tread} = \frac{K_A}{e^{-K_G T_{GA}}} e^{-K_G T_{Tread}} + G_{limit} \tag{4.12}$$

$$K_A = G_{TA} - G_{limit} \tag{4.13}$$

$$K_G = \frac{log(K_A) - log(K_B)}{T_{GB} - T_{GA}} \tag{4.14}$$

$$K_B = G_{TB} - G_{limit} \tag{4.15}$$

where,

w_{cp} Contact patch width

G_{tread} Shear modulus of the tread

h_{tread} Thickness of the tread

G_{TA} Shear modulus at reference temperature A

G_{TB} Shear modulus at reference temperature B

G_{limit} Shear modulus at reference for infinite temperature

T_{GA} Reference temperature A

T_{GB} Reference temperature B

The sliding part of the contact patch is described by the following equation of dynamic friction coefficient. The master curve is assumed to have a Gaussian shape, where v_s is the sliding velocity and T_{tread} is the tread temperature.

$$\mu_{mc} = \mu_{base} + (\mu_{peak} - \mu_{base}) e^{-(K_{shape}(log_{10}(v_s) - K_{shift}(T_{tread} - T_{REF})))^2} \tag{4.16}$$

Although no direct reference is made, it is understood that this equation is based on Savkoor's friction law [14]. Further investigation leads us through references by Grosch [15] to this friction law. It can be seen that equation 4.16 takes it into account the relation between the effect of velocity and the effect of temperature on the visco-elastic properties of rubber as proposed by William, Landel and Ferry [16]. The WLF equation is simplified to:

$$log a_T = -K_{shift}(T_{tread} - T_{REF}) \tag{4.17}$$

The pressure dependency of the friction is assumed to reduce linearly with increase in contact patch pressure.

$$P_{cp} = \frac{F_z}{A_{cp}} \tag{4.18}$$

$$K_{cpp} = 1.0 - K_{pcpp}\frac{P_{cp}}{K_{refcpp}} \tag{4.19}$$

$$\mu_d = K_{cpp}\mu_{mc} \tag{4.20}$$

$$\mu_0 = K_{cpp}\mu_{ref} \tag{4.21}$$

Thermal Model

For the thermal model, a lumped parameter approach is used that consists of three bodies, namely, the tread with temperature T_{tread}, the carcass with temperature $T_{carcass}$ and the inflation gas with temperature T_{gas}. A schematic of the model is shown in figure 4.4. The track surface with surrounding air provides the boundary conditions with fixed

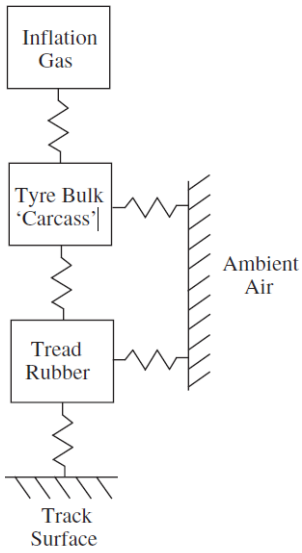

Figure 4.4: Schematic of the Thermal Model of Kelly and Sharp

temperatures T_{road} and T_{amb}. In contrast to the study of Fevrier and Le Maitre [17], the tread has a single temperature value and thus does not compute a complex temperature profile across the contact patch area. The temperature change of the three bodies is governed by the following differential equations.

$$\dot{T}_{tread} = \frac{Q_{sliding} - Q_{tread,road} + Q_{carcass,tread} - Q_{tread,ambient}}{S_{tread}M_{tread}} \tag{4.22}$$

$$\dot{T}_{carcass} = \frac{Q_{damping} - Q_{carcass,tread} - Q_{carcass,ambient} - Q_{carcass,gas}}{S_{bulk}M_{bulk}} \tag{4.23}$$

$$\dot{T}_{gas} = \frac{Q_{carcass,gas}}{S_{gas}M_{gas}} \tag{4.24}$$

There are two heat generation processes considered:

- work done on the tread rubber due to carcass deflection
- friction in the sliding region of the contact patch

Apart from the heat generation, there are four types of heat transfers that are considered.

- Heat transfer with the ambient air
- Heat transfer between the tread and carcass.
- Heat transfer between tread and road.
- Heat transfer between the carcass and inflation gas.

In racing involving outboard mounted carbon brakes, a significant amount of heat can also be contributed to the tyre and rim by radiation from the brake disc, but this is not included.
The volume occupied by the inflation gas is assumed to be constant. The tyre pressure is set at the start of a simulation to a given value at a given gas temperature. The mass of gas in the tyre is computed at this point and used for all subsequent pressure calculations. The gas pressure is computed from the gas temperature, mass and volume using the ideal gas law.

4.3 Proposed Thermal Model

In the previous sections, some benchmark thermal models were discussed. However, there were still some improvements or modifications that can be done on these models to improve their accuracy or make more physical sense.
As mentioned in section 4.2.1, the heat transfer between the road and the tread was not considered in the original equations of Model 2. For the final results, this heat transfer term was added to the differential equations to improve the accuracy of the thermal model as also pointed out in the work of S. van Rijk [18]. The modified equations are described below.

$$C_{eq\_carcass}\frac{dT_{carcass}}{dt} = P_{rolling\_resistance} + P_{cond} + P_{ambient,carcass} \tag{4.25}$$

$$C_{eq\_tread}\frac{dT_{tread}}{dt} = P_{Fx\_tyre} + P_{Fy\_tyre} - P_{cond} + P_{ambient,tread} + P_{cond,road} \tag{4.26}$$

where,

$$P_{cond,road} = H_{tread,road}(T_{tread} - T_{road}) \tag{4.27}$$

For the thermal model from Kelly and Sharp, the dynamic friction values were used from the measurements data to best optimize the model. However, in a simulation model, the dynamic friction is unknown and thus the friction model from Kelly and Sharp is modified to also account for the shift along the μ axis with compound temperature. The idea is taken from the work done by Abolhasen et al [19] where the parameters of the friction models from Savkoor [14] and Heumer [20] are made temperature dependent.

A similar concept is applied to the dynamic friction model used by Kelly and Sharp. The final equations for the dynamic friction model are described below. The equation uses the basic friction model from Savkoor with shift along the frequency axis due to

temperature using the equation from Kelly and Sharp and finally the shift along μ axis given by making parameters μ and h temperature dependent.

$$\mu_d(T) = \mu_{base} + (\mu_{peak}(T) - \mu_{base})e^{-(h(t)(log_{10}(\frac{v_s}{V_{max}}) - K_{shift}(T_{tread} - T_{REF})))^2} \tag{4.28}$$

where,

$$\mu_{peak}(T) = a_1 T^2 + a_2 T + a_3 \tag{4.29}$$

$$h(T) = b_1 \frac{e^{b_2 T_{tread}}}{e^{b_2 T_{ref}}} \tag{4.30}$$

The implications of this equation is that it captures the affects of both sliding and non-sliding friction components. The change in the parameter h changes the slope of the μ curve, which in physical terms relates to the change of shear modulus of the tyre compound with temperature. As the name suggests μ_{peak} relates to the peak friction properties of the tyre compound with change in temperature. The constants for both these parameters can be identified using measurement data. A comparison of the μ derived from the model and from the measurements is shown in figure 4.5.

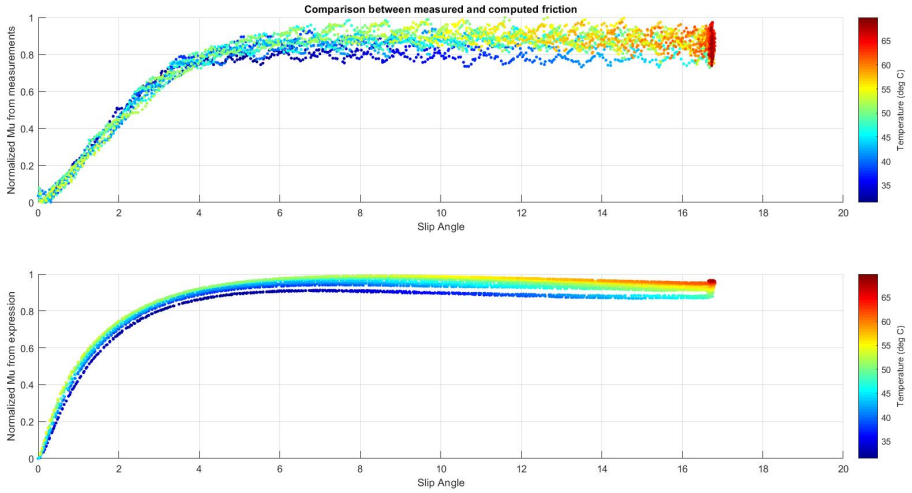

Figure 4.5: Comparison between modified friction model and measurement data

The final equations for the thermal model used are that from the thermal model developed by Kelly and Sharp with the modified μ equation described in equation 4.28.

4.4 Results

The results from the thermal models developed were compared with actual measurement results for pure braking, acceleration and lateral tests. After the model was developed, the initial values of coefficients were taken from the work done by S. van Rijk [18] and Kelly and Sharp [13]. These were then further tuned using optimization with bounds on the parameter values.

For tuning the parameters, a non-linear least square method is used to give a good

approximation of the temperatures. The method optimizes according to the error from the measurements defined by:

$$\epsilon = 100\% \sqrt{\frac{\Sigma(T_{model} - T_{meas})^2}{\Sigma T_{model}^2}} \tag{4.31}$$

It was also checked that the fit provides good estimation for different manoeuvres. For example, the parameters were first optimized for lateral sweeps and then checked again for acceleration runs. This way an average was taken for the parameters to get a better fit throughout the driving envelope.
Figure 4.6 shows the comparison between the measured temperature values and the temperature obtained from the thermal model.

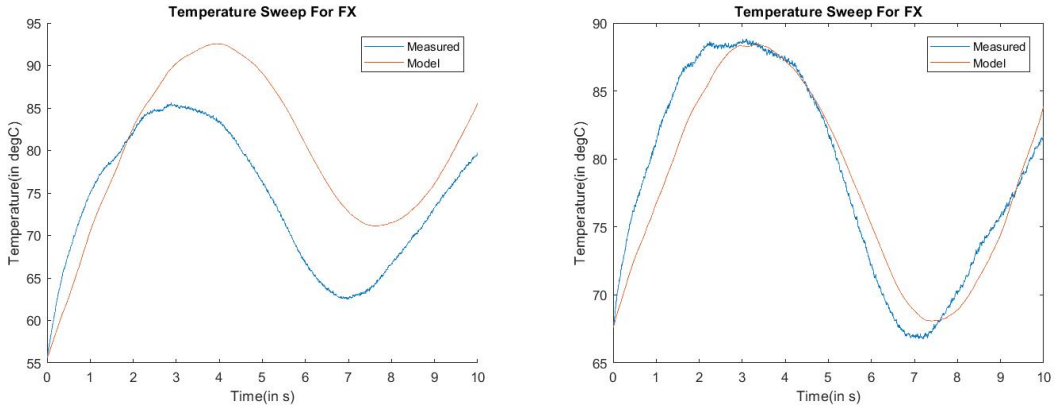

(a) Results of the model by Kelly and Sharp (b) Results of the proposed thermal model

Figure 4.6: Temperature comparison for braking measurements

The error achieved for different thermal models are summarized in table 4.1. It can be seen that the modified thermal model provides good fits for all types of manoeuvres. Also, from the table it is not clear about the adaptation of these models to measurements with different normal loads. The models were checked for the errors using different measurement data and it was found that although the model by Aldo Sorniotti has a good fit for a particular measurement, the error increases when the conditions change as can be seen in figure 4.7.

	Model by Aldo Sorniotti	**Model from Kelly and Sharp**	**Modified Thermal Model**
Pure braking	**2.5 %**	10 %	2.9 %
Pure Cornering	3.2 %	2.99 %	**2.65 %**
Pure Acceleration	5.2 %	**4.7 %**	5.5 %

Table 4.1: Error achieved by different thermal models

However, since the proposed model based on Kelly and Sharp takes into account the contact patch area which is dependent on both the normal load and the air pressure, it can easily adapt to different measurements and the maximum error is limited to around 6%.

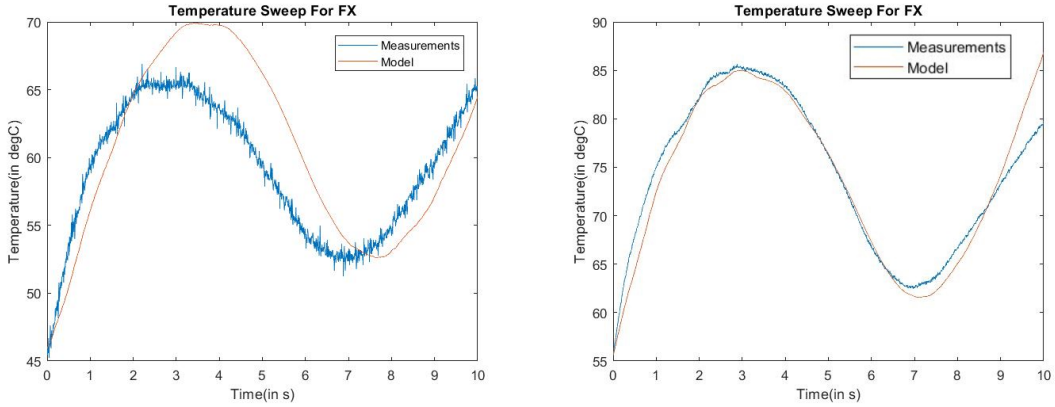

(a) Average Fz = 600N (b) Average Fz = 1000N

Figure 4.7: Temperature comparison for Model by Aldo

4.5 Summary

The different thermal models which can be used in a full car model were discussed. Initially, some thermal models from literature developed by Aldo Sorniotti and Kelly and Sharp were presented. There were modifications proposed for both these models to improve the accuracy. A term related to conduction of heat to the road was added in the heat equations used by Aldo. For the model from Kelly and Sharp, a new equation for dynamic friction coefficient was proposed. The results of the benchmark models were then compared with the modified model and it was seen that the modified model performs better under varying conditions of the tyre. The thermal model will now be coupled to a tyre model to affect the force produced with different tread temperatures.

CHAPTER 5

STEADY STATE TYRE MODEL

5.1 Introduction

This chapter describes the tyre model used to calculate the steady state forces in the simulations. For the basic simulations, the tyre model based on the magic formula developed by Pacejka et al. [21] is used. The magic formula is then modified to incorporate the effects of tyre temperature on the force-producing capabilities of the tyre. Since, the magic formula is an empirical model, the coefficients for the model were fitted using measurement data. The performance of the modified tyre model is then compared with the measurement data and the effects are explained.

It should be noted that the expressions mentioned in this chapter are for steady state conditions and considers the basic equations developed by Pacejka et al [21]. The modifications are also shown on this basic equation. However, in the actual model the equations are more detailed and include the effects of load, camber, pressure etc.

5.2 Baseline MF

5.2.1 Introduction

The magic formula is one of the empirical models which is widely used to calculate steady-state tyre force and moment characteristics to be used in vehicle dynamic studies. This model was developed by E.Bakker, H. B. Pacejka and L. Lidner. It uses a special function to represent measurements instead of tables or polynomial functions. By changing the coefficients of the function, the same general function can be used for lateral forces, longitudinal forces and self-aligning torque.

5.2.2 General Expression

The special function referred to in the introduction has the following form:

$$y(x) = D\sin(C\arctan Bx - E(Bx - \arctan Bx)) \tag{5.1}$$

$$Y(x) = y(x) + S_v \tag{5.2}$$

$$x = X + S_h \tag{5.3}$$

Y(X) may represent side force, longitudinal force or self-aligning torque. X denotes slip angle α or longitudinal slip κ. The remaining variables of the Magic Formula describe

the following coefficients:

B	stiffness factor
C	shape factor
D	peak factor
E	curvature factor
S_h	horizontal shift
S_v	vertical shift

The Magic formula y(x) typically produces a curve that passes through the origin x = y = 0, reaches a maximum and subsequently tends to a horizontal asymptote. For given values of the coefficients B, C, D and E the curve shows an anti-symmetric shape with respect to the origin. The shifts S_h and S_v have been introduced to allow for offsets with respect to origin.

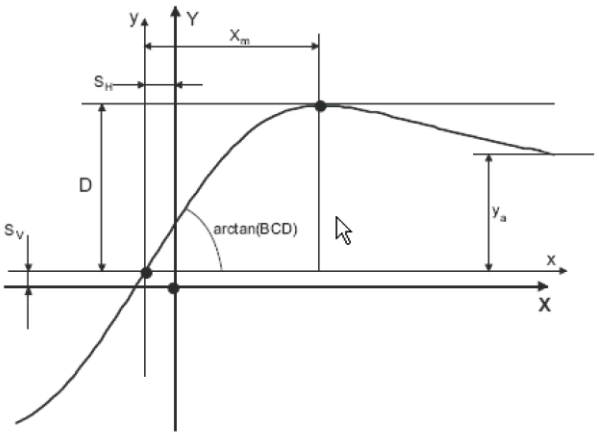

Figure 5.1: Curve produced by the general form of the Magic Formula [1]

Since, the magic formula uses a sine function, the peak value is determined by the peak factor, D. The derivative of equation 5.1 at the origin gives BCD as a result. Thus, BCD determines the stiffness of the tyre in lateral or longitudinal direction. The shape of the curve is influenced by both E and C, where E enables a local stretch or compression and C controls the extent of the sine function. It determines if the curve looks like a side force characteristic, a longitudinal force characteristic or self-aligning torque characteristic.
The parameters S_h and S_v enable the modelling the infuence of ply steer, conicity, rolling resistance and camber angles on force generation by providing horizontal and vertical shifts respectively.

A constant value of the coefficients makes the equation valid for a particular load and camber angle. Thus, the model defines the coefficients in order to add camber and load dependency.

5.3 Extended MF with Temperature Effects

As mentioned in the introduction of this chapter, the modifications made are only shown for the basic magic formula but are actually used with the extended magic formula. Similar to the equation of the dynamic friction coefficient (4.28) developed for the thermal model, the modifications for the magic formula affect the stiffness of the force curve and the peak friction achieved with reference to temperature variation.

In order to affect the performance changes a reference temperature T_{ref}, is defined where the performance is known from measurements. A delta is then defined to account for the change in temperature which is defined as shown below.

$$\Delta T = \frac{T - T_{ref}}{T_{ref}} \tag{5.4}$$

The modifications done to affect the different forces and moments due to temperature changes are described next. The performance of this model was compared with the actual measurements by comparing the normalized friction values as a function of temperature. In order to check the performance of magic formula, the temperature values from the measurements were used as an input to the model.

5.3.1 Longitudinal Force

There are 4 temperature coefficients (each for lateral and longitudinal force) defined to affect the force producing capability of the tyre. The coefficients for the temperature effects on longitudinal force are described below.

$TX1$	Linear temperature effect on slip stiffness
$TX2$	Quadratic temperature effect on slip stiffness
$TX3$	Linear temperature effect on longitudinal friction
$TX4$	Quadratic temperature effect on longitudinal friction

The coefficients defined above are used to modify the B and D factors of the magic formula to affect the slip stiffness and longitudinal friction respectively. The modifications in the longitudinal force equations are described below.

$$D_x = (1 + TX3 * \Delta T + TX4 * \Delta T^2) * D_{xbase} \tag{5.5}$$

$$K_x = (1 + TX1 * \Delta T + TX2 * \Delta T^2) * K_{xbase} \tag{5.6}$$

$$B_x = \frac{K_x}{C_x * D_x} \tag{5.7}$$

where,

D_{xbase}	Peak factor, D as defined in base magic formula for longitudinal force
K_{xbase}	K_x as defined in baseline magic formula

As can be seen in figure 5.2, the modifications are able to match the measurement data for longitudinal force. The change in slip stiffness and the longitudinal friction is observed with the change in temperature. The only difference in the plots is the disturbance seen in the measurement plot. This can be explained due to the road surface irregularities and conditions during the measurements.

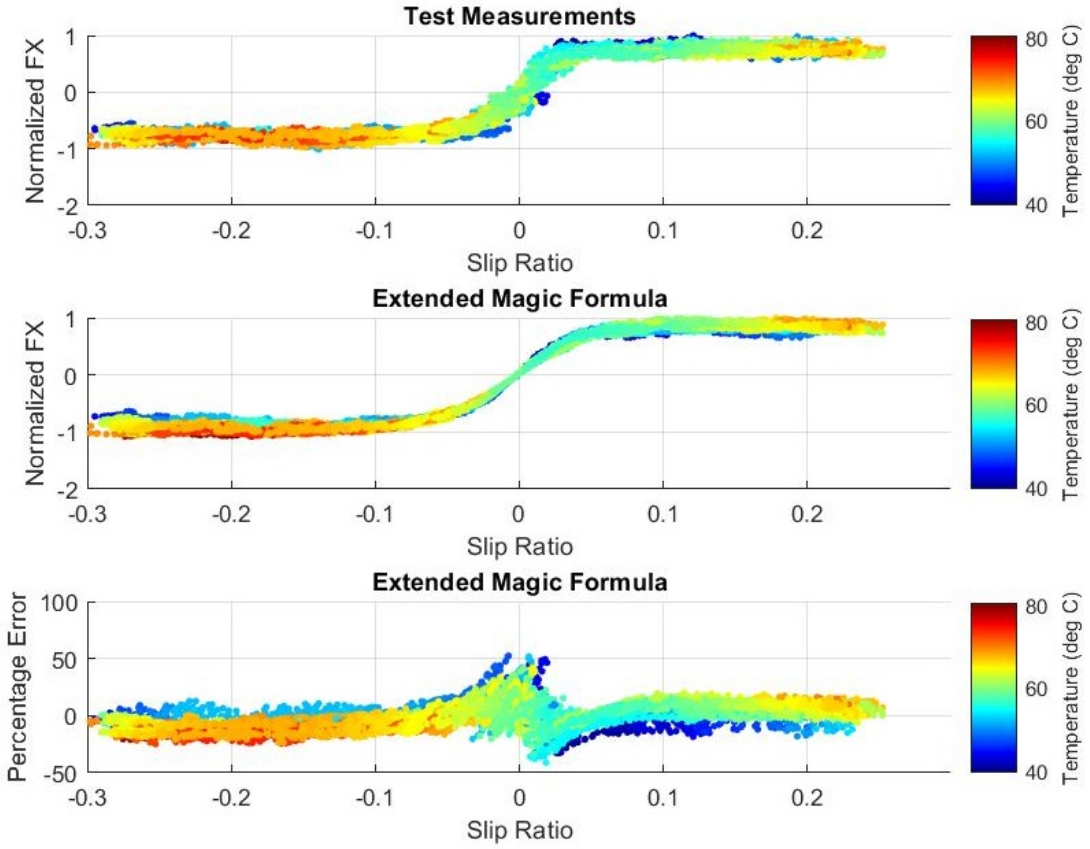

Figure 5.2: Comparison of Extended Magic formula with measurement data.

5.3.2 Lateral Force and Self-Aligning Moment

As mentioned before, there are 4 temperature coefficients defined to affect the force producing capability of the tyre. The coefficients that affect the lateral force are described below.

$TY1$	Temperature effect on cornering stiffness magnitude
$TY2$	Temperature effect on location of cornering stiffness peak
$TY3$	Linear temperature effect on lateral friction
$TY4$	Quadratic temperature effect on lateral friction

Similar to the longitudinal force, the coefficients defined above are used to modify the B and D factors of the magic formula to affect the cornering stiffness and lateral friction respectively. The modifications in the lateral force equations are described below.

$$D_y = (1 + TY3 * \Delta T + TY4 * \Delta T^2) * D_{ybase} \tag{5.8}$$

$$K_y = (1 + TY1 * \Delta T) * PKY1 * F_{z0} * \sin\left(\arctan \frac{F_z}{PKY2 * F_{z0} * (1 + TY2 * \Delta T)}\right) \tag{5.9}$$

$$B_y = \frac{K_y}{C_y * D_y} \tag{5.10}$$

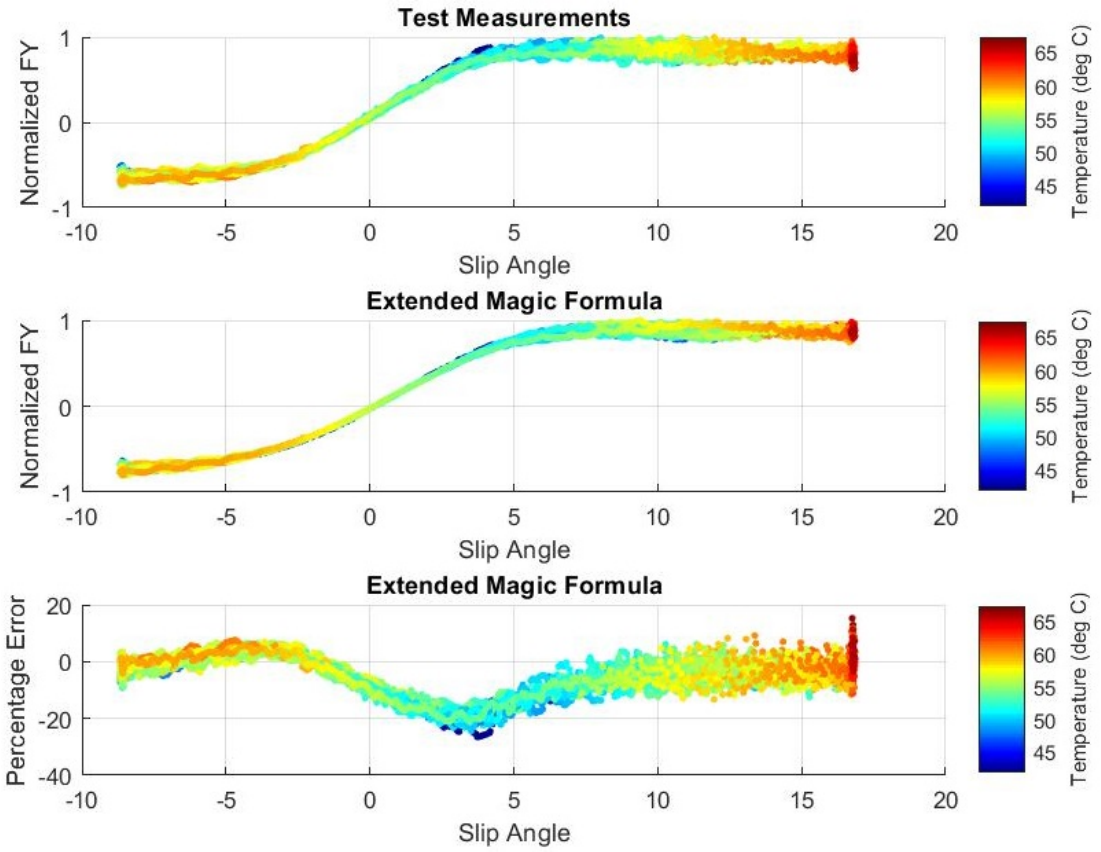

Figure 5.3: Comparison of Extended Magic formula with measurement data.

where,

D_{ybase}	Coefficient D as defined in base magic formula for lateral force
F_{z0}	Fz nominal
$PKY1$	Maximum value of stiffness Kfy/Fznom
$PKY2$	Load at which Kfy reaches maximum value

As can be seen in figure 5.3, the modified magic formula is able to match the measurement data for lateral force.
Self-Aligning Moment is defined as the product of the lateral force and the pneumatic trail of the tyre. With the same contact patch pressure distribution, the pneumatic trail would be constant and hence with temperature change the self-aligning moment will change only due to the change in lateral force. Hence, there is no need to modify the equations in the magic formula for the calculation of self-aligning moment. This can be seen in figure 5.4

5.4 Summary

The modified magic formula produces satisfactory results with varying temperature of the tread. At lower temperatures, the model results in higher tread stiffness and at higher temperatures, higher friction is achieved. The results are coherent with the physical explanation of the tyre behaviour.

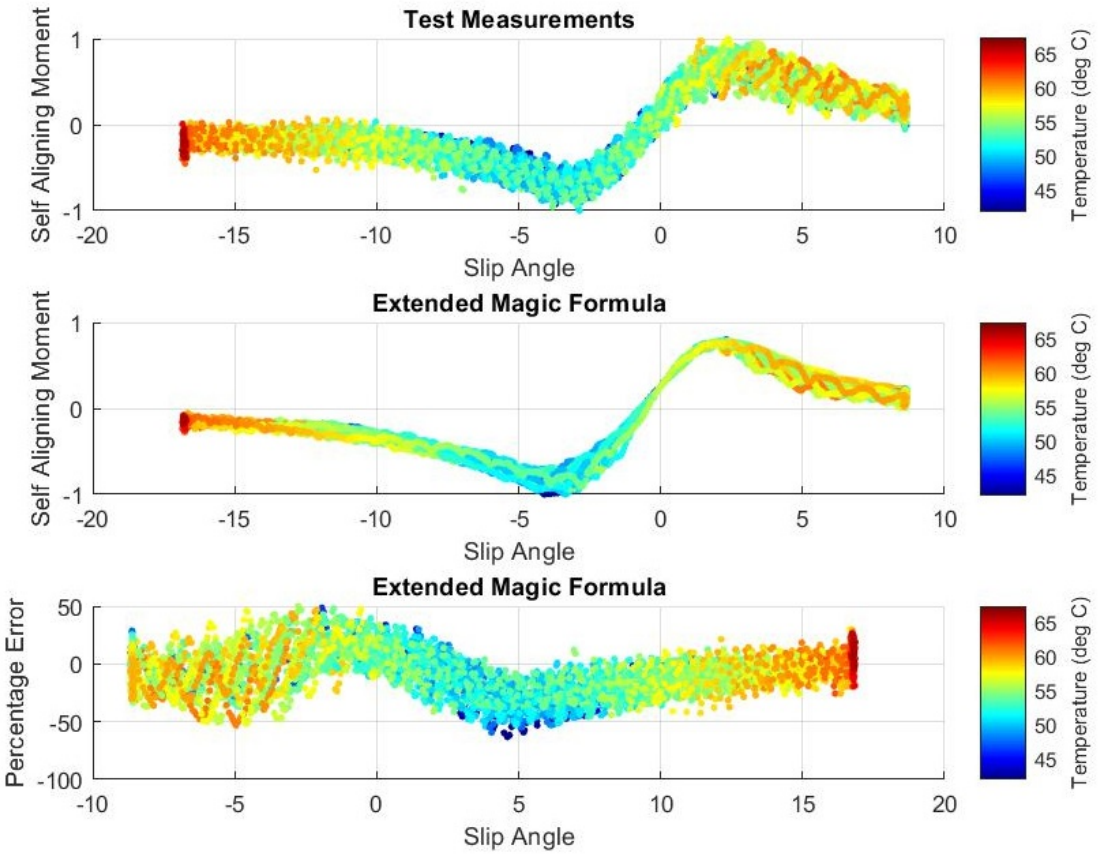

Figure 5.4: Comparison of Extended Magic formula with measurement data.

CHAPTER 6

TYRE AND CAR MODEL VALIDATION

6.1 Introduction

This chapter describes the full-vehicle model where the chassis model is coupled with the thermal model and the modified tyre model described in chapters 2, 4 and 5 respectively.

Firstly, the model inputs and outputs are defined along with the structure in which the simulation works at each time step. After the model definition, the simulation is run for different scenarios and the results are compared with data obtained from the sensors on the car. The chapter concludes with the discussion about these results and the modifications made to the parameters to account for the difference in simulation environment and real driving.

As the objective of the simulation is to match the vehicle performance obtained in real life, the inputs and outputs are similar to that obtained in an actual car. Also, it was kept in mind that the simulation could be used to tune the control systems and be further developed for SIL/HIL simulations.

6.2 Model Inputs

- Since the objective of the thesis was to make a vehicle dynamics model, the powertrain is not modelled and thus the block related to throttle input and the conversion to corresponding torque on motors is not present. Thus, the torques available at the wheels are used as inputs to the simulation. These torques act on the revolute joint between the upright and the tyres.
- The torque contains both the driving torque and regenerative braking torque. Also, the brake torque estimated based on the pressure sensor values is reduced from the overall torque.
- The other input to the simulation is the steering input from the driver. The values from the steering sensor are used and then converted to rack displacement using the rack and pinion specifications.
- For the thermal model, initial values for the tread, carcass and gas temperatures are defined along with the cold pressure of the tyres.

6.3 Model Outputs

- The full vehicle model has different sensors which correspond to the sensors available in the actual car. The first ones is the wheel rpm sensor which senses the rotational speed of the tyre.
- There are accelerometers that measure the acceleration in longitudinal and lateral direction at the centre of gravity of the chassis.
- The forward and lateral velocity of the car is also measured along with the yaw rate and the position of the car in world frame. All these sensors measure at the centre of gravity of the chassis.
- All the tyre parameters can also be seen during the simulation including the temperature and pressure profile for each tyre.

A representation of the different sensors on the actual car is represented in figure 6.1 followed by a visualization of the dual antenna speed sensor in figure 6.2.

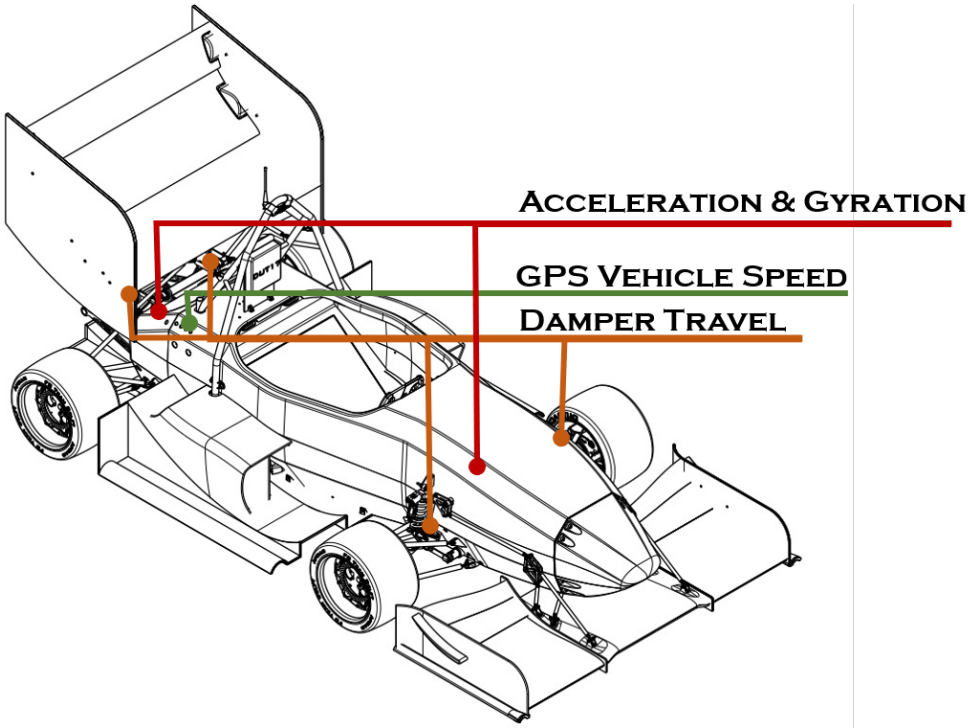

Figure 6.1: Overview of the sensor mounting positions

6.4 Model Structure

The overall structure of the simulation is as shown in figure 6.3. This is the schematic representation of the complete simulation.
For each time step, the chassis model calculates the state of the different parts of the car and passes the tyre states (position, velocity, acceleration) to the tyre model (Figure 6.4).

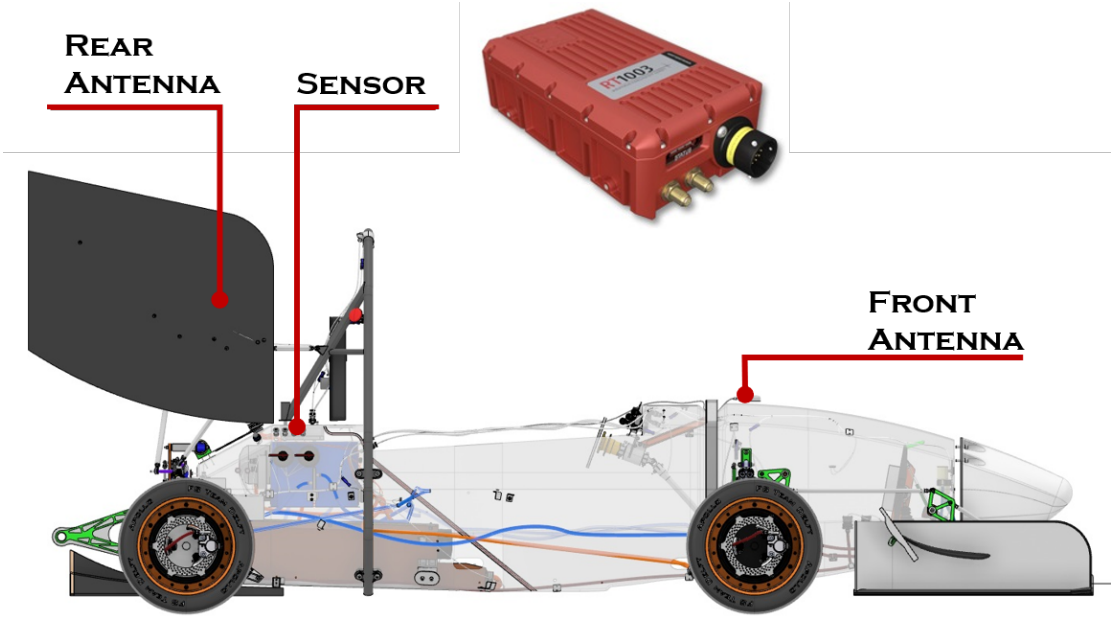

Figure 6.2: Overview of the Vehicle speed sensor

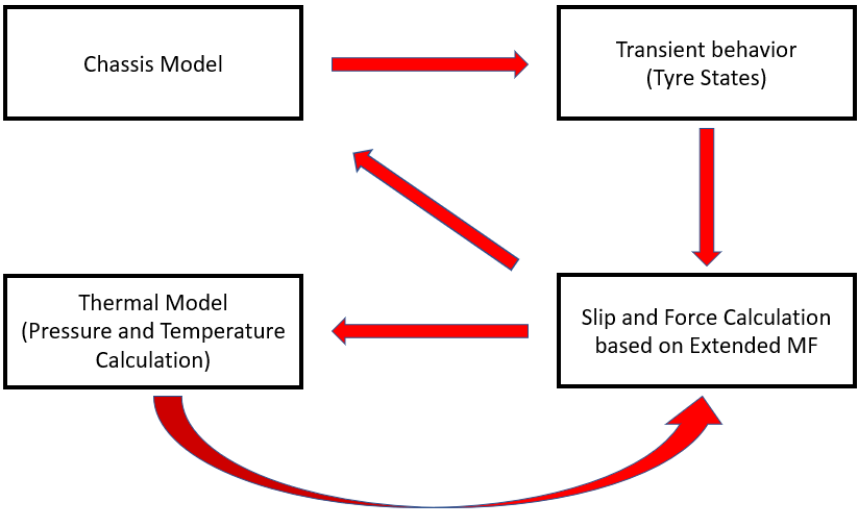

Figure 6.3: Model Structure

Based on these states, the model calculates the forces that the tyre will produce. These forces are then fed to the thermal model which calculates the temperature change due to these forces. The forces and moments are then fed back to the chassis model (Figure 6.4) and the temperature and pressure values back to the tyre model (Figure 6.5).

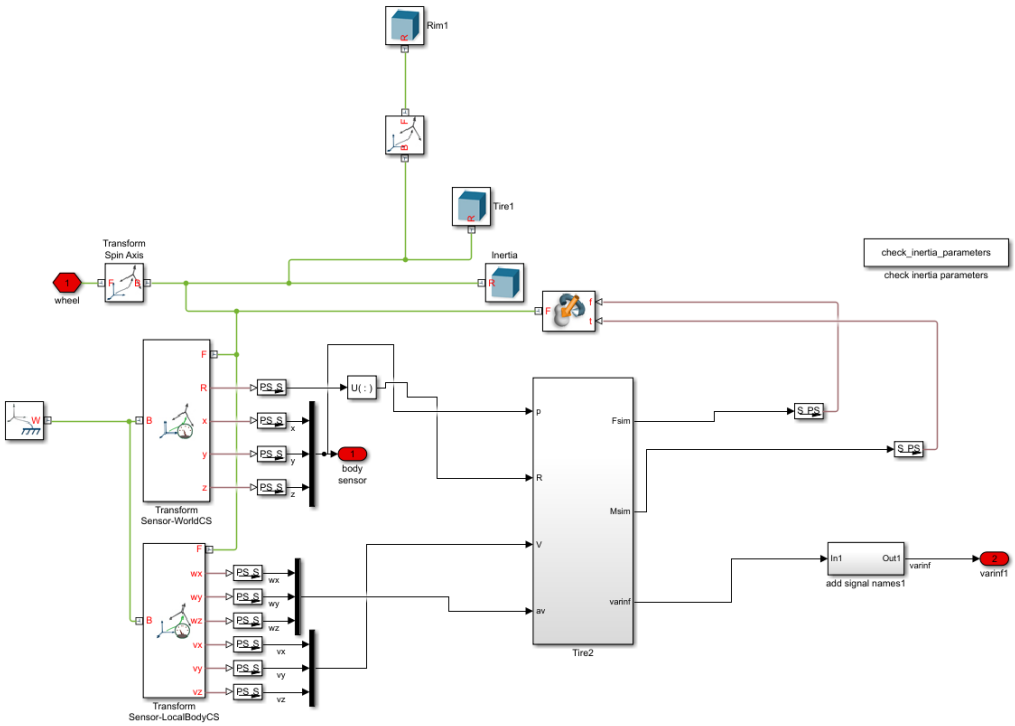

Figure 6.4: Interaction between the tyre and chassis

6.5 Model Validation

The model is validated by using 2 sets of data from the vehicle. The first simulation corresponds to a skidpad run which is used in the Formula Student competition to measure a car's steady state lateral behaviour. The other simulation performed was for a longer time and corresponds to a full lap manoeuvre.

As mentioned in the introduction of the chapter, to compensate for the differences in simulation and real driving certain changes were made which are described below.

- The first difference is the road surface, which is considered flat in the simulation as compared to a track which is bumpy and has elevation changes. Also, the friction in the transmission and bearings was not modelled initially. The effect of this difference was that for the same torque the vehicle was reaching higher velocities in the simulation as compared to the real car. In order to compensate this error, a damping value was introduced in the revolute joints between the upright and the tyre. The value was quantified with the full-lap simulation where there was little or no elevation change and the only difference was the road irregularity and friction in the transmission.
- The second difference was in the steering input. In the real car, there is compliance in the system which leads to a lower steering ratio. This was quantified using the skidpad simulation, since the track layout is known and the position of the car in the simulation was measured.

The results of these simulations are discussed next and the differences explained.

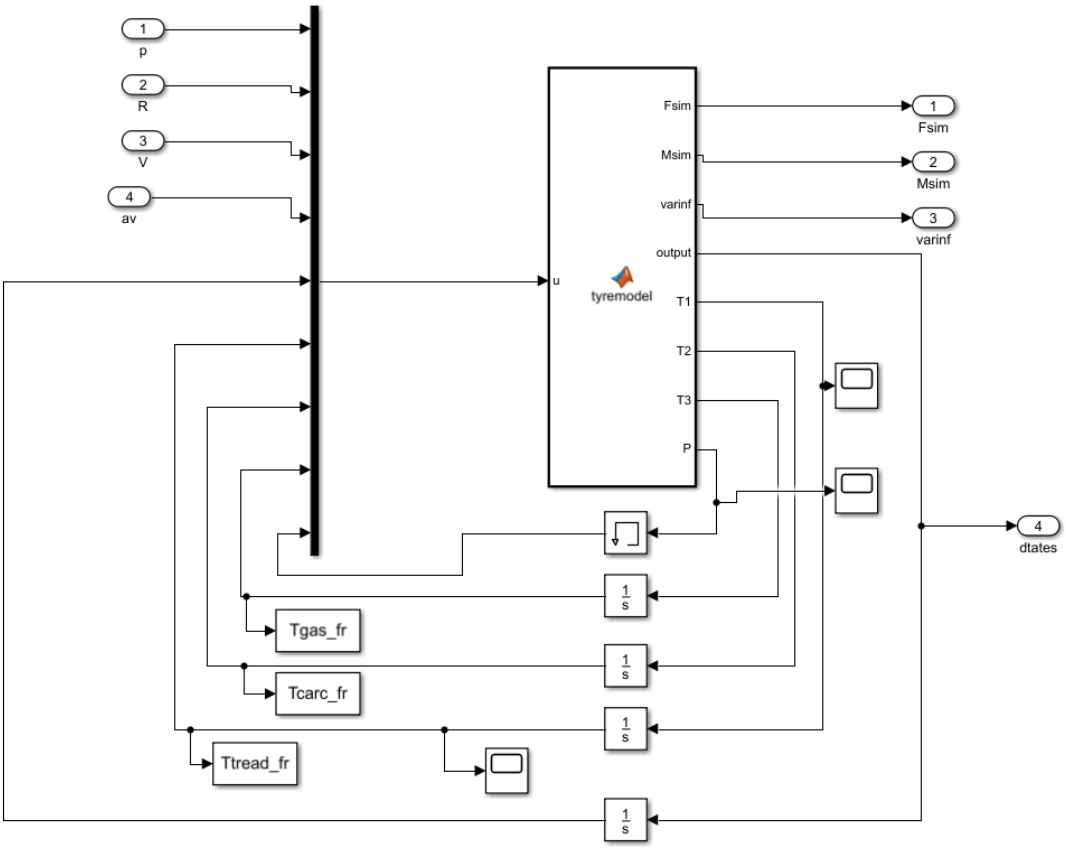

Figure 6.5: Updated temperature and pressure values fed to the tyre model

6.5.1 Skid-pad Simulation

The skidpad course consists of two pairs of concentric circles in a figure of eight pattern. A schematic overview of the track is shown in figure 6.6 [22]. The centres of these circles are 18.25 m apart. The inner circles are 15.25 m in diameter and the outer circles are 21.25 m in diameter. The driving path is the 3 m wide path between the inner and the outer circles.

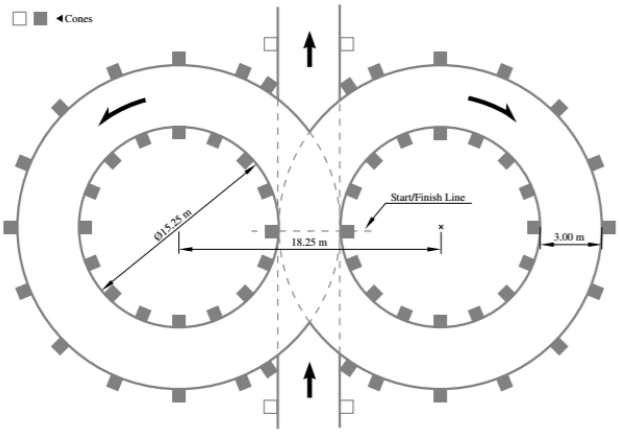

Figure 6.6: Skidpad track layout

A correct skidpad run is performed in the following way: The vehicle will enter perpendicular to the figure of eight and will take one full lap on the right circle to establish the turn. The next lap will be on the right circle and will be timed. Immediately following the second lap, the vehicle will enter the left circle for the third lap. The fourth lap will be on the left circle and will be timed. Immediately upon finishing the fourth lap, the vehicle will exit the track perpendicular to the figure of eight moving in the same direction as entered.
The goal of the skidpad event is to cover the second and fourth lap as fast as possible. In order to do this as fast as possible the lateral forces generated by the tyre-road friction should be as big as possible.
The comparison of the velocity and wheel speeds of the vehicle from sensors on the car and the simulation is shown in figure 6.7.

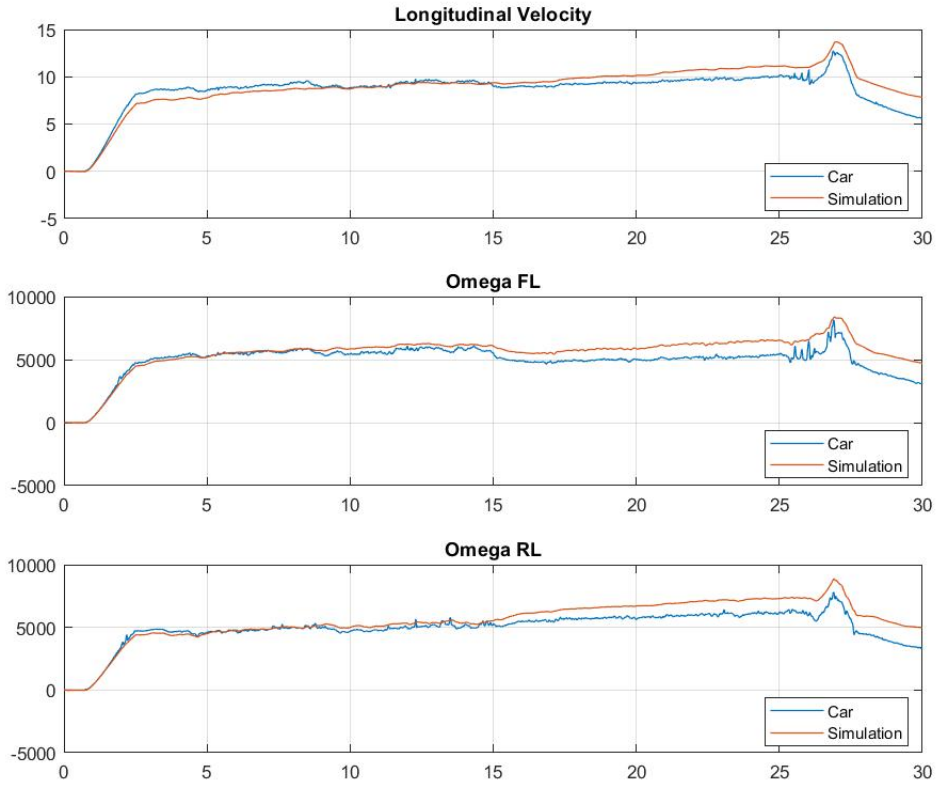

Figure 6.7: Skidpad Simulation - velocity and wheel speeds comparison with actual car

In order to compare the results, the data from the car was filtered using a Savitzky–Golay filter in matlab. It is a digital filter that can be applied to a set of digital data points for the purpose of smoothing the data, that is, to increase the signal-to-noise ratio without greatly distorting the signal. This is achieved, in a process known as convolution, by fitting successive sub-sets of adjacent data points with a low-degree polynomial by the method of linear least squares.
The filtered data was then used to validate the simulation results. The root mean square errors for the accelerations and yaw rate is presented in table 6.1. The comparison of the accelerations and yaw rate of the vehicle is shown in figure 6.9a. Also, the absolute error

and RMS error is shown in figure 6.9b.

	Root mean Square Error
Longitudinal Acceleration	0.65 m/s^2
Lateral Acceleration	1.26 m/s^2
Yaw Rate	0.162 rad/s

Table 6.1: Root mean square error for Skidpad simulation

As can be seen in figure 6.9a, the simulation produces an oversteered car as compared to the data from sensors on the car. This difference can be related to the roll stiffness of the chassis. The chassis is modelled as a rigid body and thus is infinitely stiff in the simulations as compared to a chassis with limited roll stiffness. This leads to higher yaw rates in the simulation and thus an increase in the RMSE for the yaw rate.

Also, it can be seen that the accelerations and yaw rate matches the car data better in the left turn circles. This can be due to the elevation change in the skidpad circuit which affects the accelerometer readings. It can also be seen in the velocity and wheel speed plots. The difference in the speed increases in the second half of the simulation. The evolution of tyre temperature is also shown in figure 6.8. As can be seen in the figure, the outer tyres (initially left tyres for the right turn) start heating up first due to higher normal loads and thus higher force generation or higher friction. As soon as the car changes direction, the right tyres start heating up which is as expected.

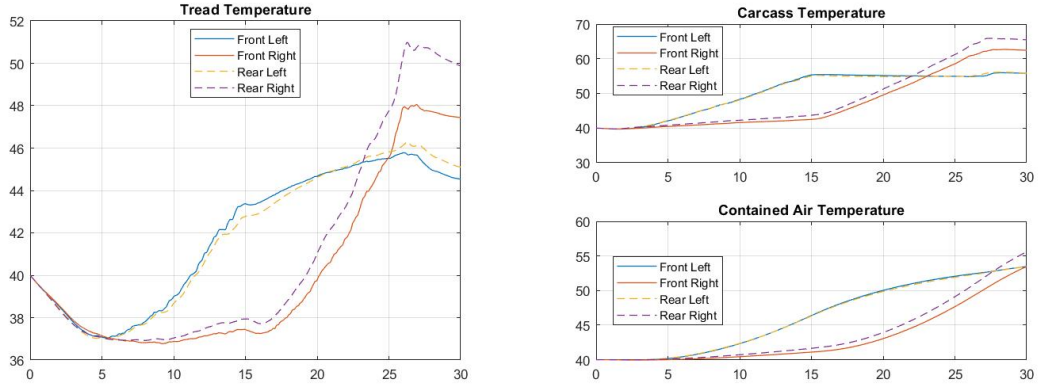

(a) Tyre Tread Temperature

(b) Tyre Carcass and Gas Temperature

Figure 6.8: Evolution of Tyre temperatures

6.5.2 Full Lap Simulation

In order to check the simulation for transient behaviour, a full lap simulation was performed. The data for the simulation was taken from one of the Endurance runs, where the car does 22km of driving or 18-20 laps. The simulation is done for 50 seconds which relates to around 1 km or 1 lap of the circuit. For the full-lap simulation, brake torques are also added to the wheel torque since the mechanical braking is dominant for a fast lap as compared to skidpad where there is only regenerative braking. The parameters for

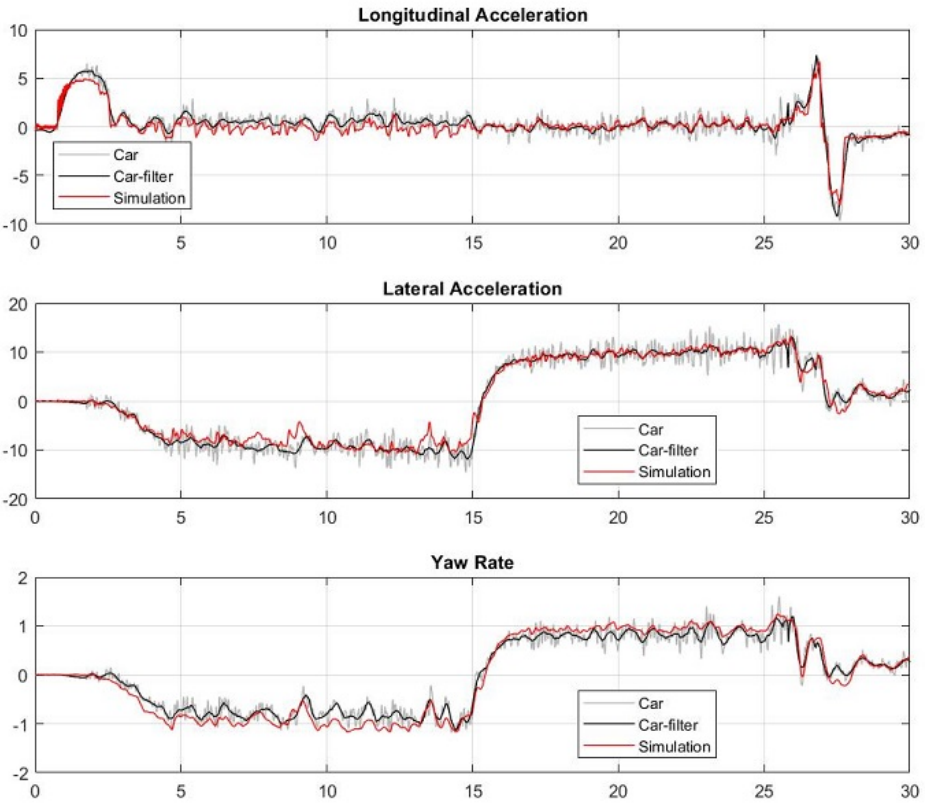

(a) Accelerations and Yaw rate

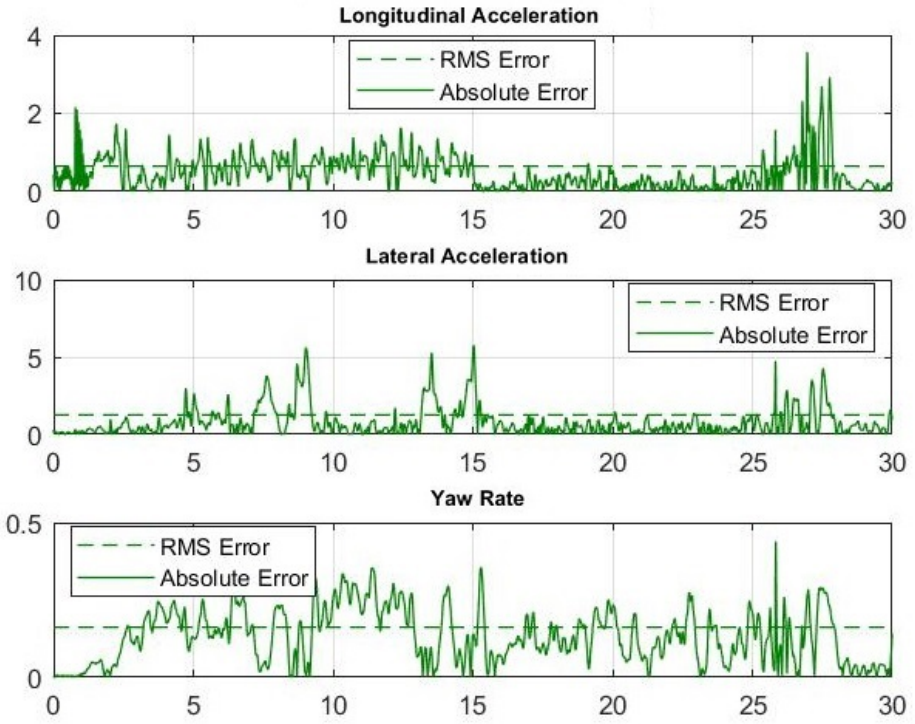

(b) Absolute and RMS Error

Figure 6.9: Skidpad Simulation Validation

the full lap simulation and the calculations done to convert the brake pressure to braking torque is shown in appendix A.

Endurance event is combined with the efficiency event. The goal of the event is to score the maximum points while optimizing between performance or lap times and the efficiency of the car. The endurance track layout is a closed lap circuit built to the following guidelines:

- Straights: No longer than 80m
- Constant Turns: up to 50m diameter
- Hairpin Turns: Minimum of 9m outside diameter (of the turn)
- Slaloms: Cones in a straight line with 9m to 15m spacing
- Miscellaneous: Chicanes, multiple turns, decreasing radius turns, etc.
- The minimum track width is 3m

The comparison of the velocity and wheel speeds of the vehicle from sensors on the car and the simulation is shown in figure 6.10. There is some difference in the velocity and

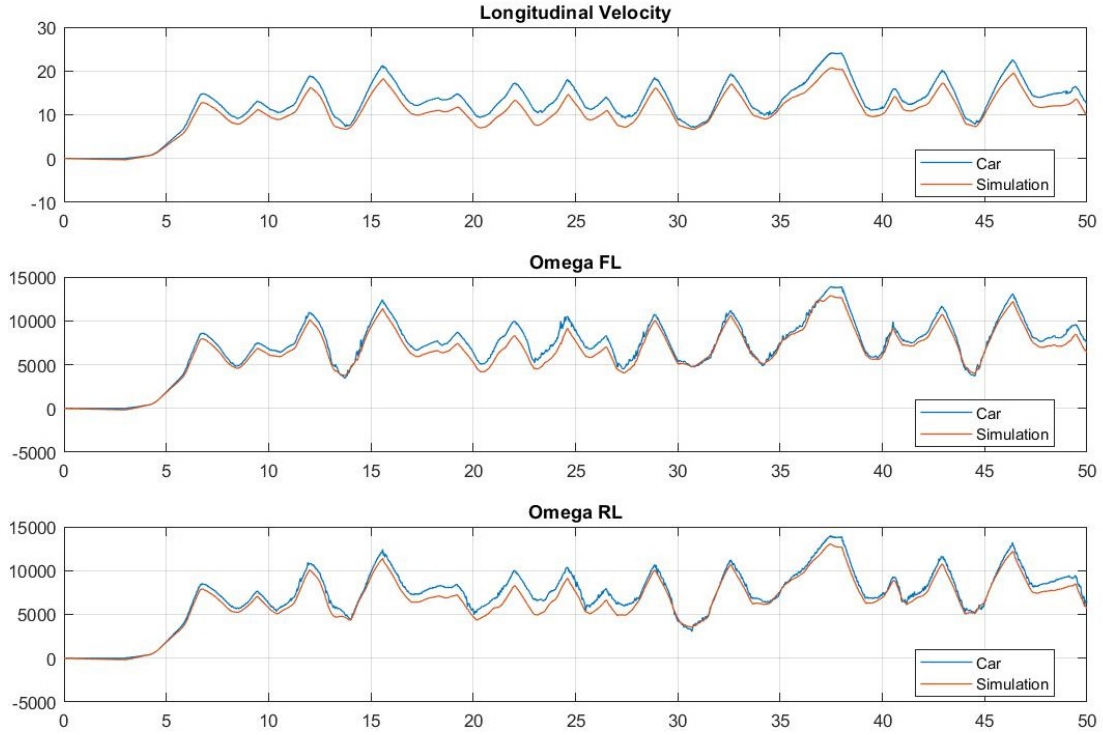

Figure 6.10: Full-Lap Simulation - velocity and wheel speeds comparison with actual car

the wheel speeds obtained in the simulation and the actual car. This difference can be explained by the estimated friction coefficient between the brake disc and brake pads. The actual friction in the brake system is non-linear, however, for simplicity a constant values is used in the simulation to calculate the brake torque from pressure sensor values.

Again, in order to compare the accelerations and yaw rate, the data from the car was filtered and the RMSE was calculated from the filtered data. The RMSE for the accelerations and yaw rate for the full-lap simulation is provided in table 6.2. The comparison of the results are shown in figure 6.12a and the absolute error in figure 6.12b. It can be seen in the results that the yaw rate from the simulation matches the car data

	Root mean Square Error
Longitudinal Acceleration	1.425 m/s^2
Lateral Acceleration	3.19 m/s^2
Yaw Rate	0.158 rad/s

Table 6.2: Root mean square error for Full-Lap simulation

quite well. This means that the behaviour of the car in the simulation relates to the actual car even in transient conditions. However, as stated in the previous section, there was a difference in the chassis roll stiffness. To counteract the change in behaviour, the ARB stiffness was tuned to get the correct vehicle behaviour.

The RMSE for longitudinal acceleration is also a bit higher as compared to the skidpad simulation. However, the longitudinal acceleration in skidpad was very low as compared to a full-lap. Again, the simulation matches the longitudinal acceleration quite accurately.

The highest peak in error was found in lateral acceleration where the RMSE jumped to 3.19 m/s^2. The probable reasons for this increase in error can be owed to effect of camber on lateral force. The tyres were only tested for pure slip conditions and thus the coefficients for the combined slip behaviour are estimated based on similar sized formula student tyres. The effect of camber on lateral force and self-aligning moment is also unknown which would produce additional lateral force. The maximum error also occurs in a corner where the tyres are cambered due to chassis roll and are in combined slip conditions which confirms the suspicion.

The evolution of tyre temperature is also shown in figure 6.11. The results shows that the temperature of the tread steadily increases and drops a bit with straights or long corners. It can also be seen that the right tyres reach a higher temperature as compared to the left tyres. This can be explained by the circuit orientation where the car moves in an anti-clockwise direction leading to heavier loads on the right tyres for more time. The carcass gets heated up due to the deflections occurring in the tyre due to force generation. This in turn heats up the gas contained in the tyre.

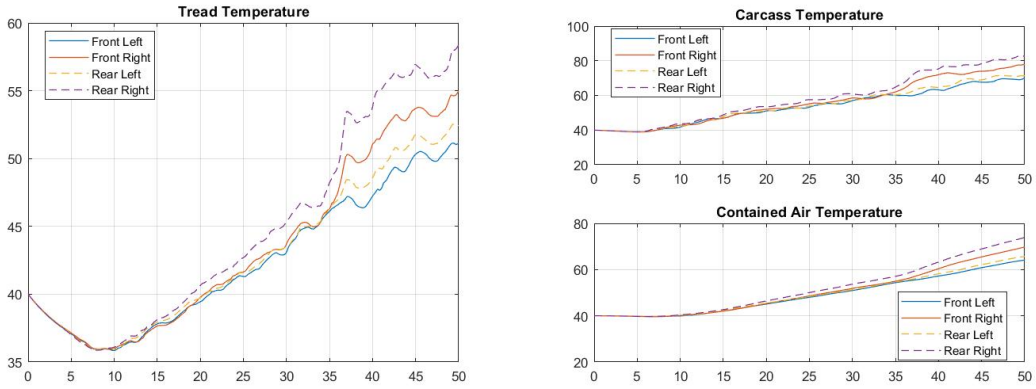

(a) Tyre Tread Temperature (b) Tyre Carcass and Gas Temperature

Figure 6.11: Evolution of Tyre temperatures in Full-lap simulation

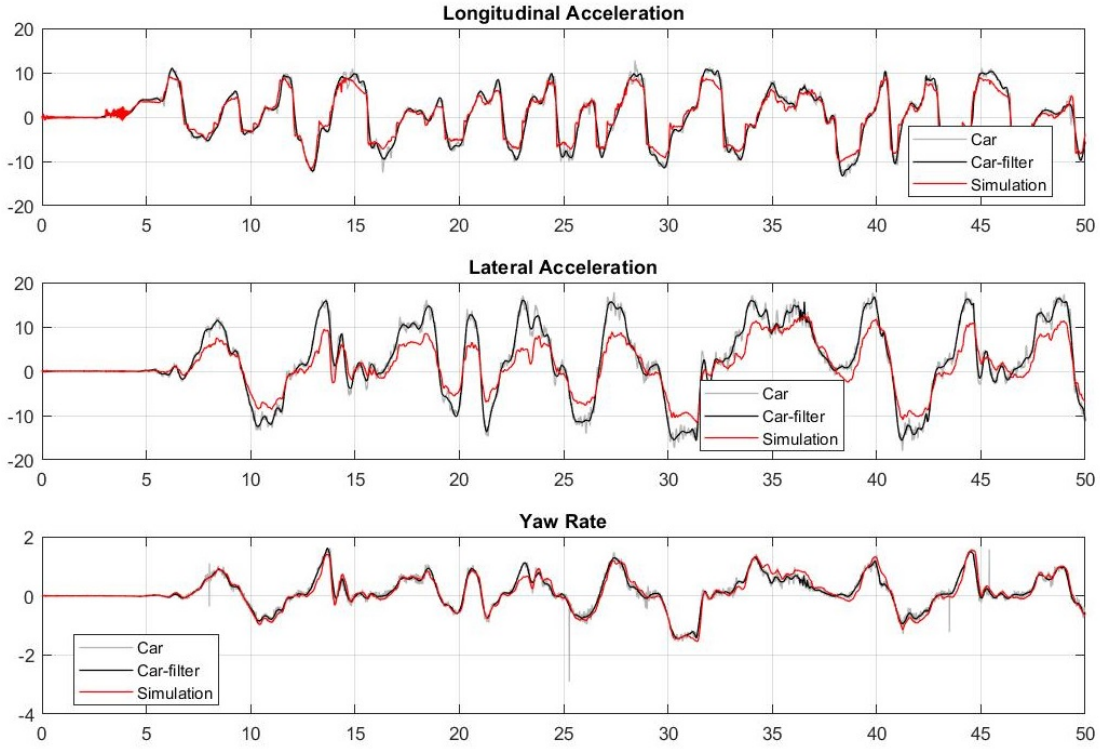

(a) Accelerations and Yaw rate

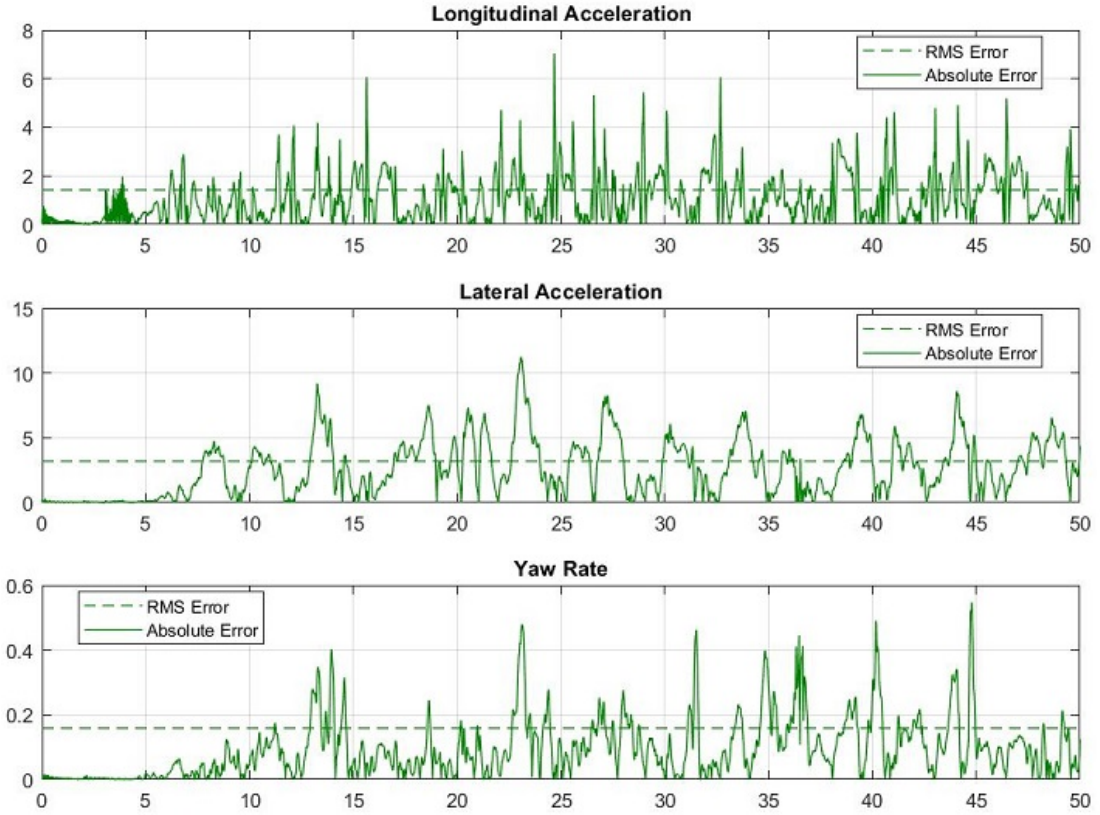

(b) Absolute and RMS Error

Figure 6.12: Full-Lap Simulation Validation

CHAPTER 7

CONCLUSIONS AND RECOMMENDATIONS

The aim of the thesis was to develop a full car vehicle dynamics model which accurately represents the actual behaviour of the vehicle. A multibody model was developed to model the chassis system. This chassis system consists of the suspension, steering, anti roll bars and chassis body. These were coupled using multibody joints which were also used as sensors or actuators.

The inputs for the multibody model consisted of inertia and mass properties from CAD (some were estimated using simple calculations) and the torques on the wheel and steering values from the data acquisition system of the car. Aerodynamic forces were applied at the static center of pressure found using CFD simulations. To improve the accuracy of the model, friction in the wheel bearings and transmission was modelled as damping in the revolute joint.

The other subsystem of tyres was modelled using the magic formula. The tyres were first tested for pure slip conditions and the parameters of the magic formula then fitted using MF Tool after post-processing the measurement data for drift and outliers. A thermal model was then proposed which made certain alterations to the thermal model from Kelly and Sharp. The proposed thermal model uses an equation for the dynamic friction coefficient which is temperature dependent. This equation takes into account the effect of sliding velocity and temperature by providing a shift of the master curve in both sliding velocity and temperature axis.

Finally, the thermal model was coupled with the magic formula to incorporate the effect of temperature on the performance of the tyres. Using the complete model, steady state and transient simulations were performed and the performance was compared with the data recorded by the DAQ from the actual vehicle.

7.1 Conclusions

Based on the work done and analyzing the data, the following conclusions can be made on developing the model and the results.

- The tyre was tested and modelled for steady state conditions by optimizing the parameters for the Magic Formula.
- An alternate thermal model was proposed that modelled a dynamic friction curve which introduces a change in peak friction and also a change in the shear modulus of

the tyre with change in temperature. This allows for a better fit of the temperature change under different conditions as the thermal behaviour is modelled using higher number of parameters.

- The thermal model was then coupled with Pacejka's magic formula to incorporate a change in the force-producing capability of the tyre with change in temperature. The magic formula was extended for these changes by introducing new coefficients that allows for the change in stiffness and peak factors. The extended magic formula was able to match the change in forces with temperature as compared to the tests performed with the tyre. A few errors were observed when comparing with the measurement data which can be linked to a high variation in the measurement runs.
- The different models were integrated to complete the model and steady-state and transient simulations were performed. A steady state lateral simulation was performed by simulating the car in a skidpad track. While for the transient simulation, a full lap of the endurance was run to check the performance. The inputs and outputs of the simulation were defined and the model was validated with the data from the DUT17.
- It was found that there were still some errors in the simulation due to estimated parameters or different track conditions. This included the effects of compliance in the system, elevation change and road irregularities, dynamic center of pressure location and tyre behaviour in combined slip conditions.
- Even with the errors, the simulation matches the behaviour of the actual car and can be used to develop control systems and understand the effects of different parameters on the behaviour or performance of the car.

7.2 Recommendations

In order to further develop the model, knowledge on multibody systems is required along with experience with the simscape toolbox of Matlab & Simulink. The model can be further extended to perform SIL/HIL simulations. This would require to model the electric powertrain, ECU and control systems in the model.

The other improvement can be made by further testing the tyres. There are some suggestions, including, but not limited to the following.

- Combined Slip conditions
- Camber influence on performance
- Pressure influence
- Rolling resistance
- Overturning Moment
- Relaxation Behaviour

This will help in better defining the parameters for the magic formula and thus improve the tyre model. The other improvement in the tyres can be made by modelling the wear

of the tyres and combine it with the thermal model. The pressure, wear and temperature have a big influence on the racing tyres and their performance.

To improve the chassis model, the inertia of the chassis should be tested along with the center of gravity height. These parameters can also have a huge impact on the performance of the simulation. Other improvements can be made by introducing road profiles and compliance in the system or the use of flexible bodies. The aerodynamic forces can be modelled better by using dynamic center of pressure locations or if possible dynamic lift and drag coefficients. Lastly, the influence of different assumptions should be looked upon and checked if the model can be expanded to exclude one of them.

APPENDIX A

SIMULATION PARAMETERS

```
%% load parameters for multibody
clear all
close all
clc
%%
ClA = 3.5;          %Lift coefficient
CdA = 1.53; %add a factor for drs in acceleration
rho = 1.225;
%Tire
par.Reff     = 0.168;              % wheel effective radius, m
par.RL       = 0.200;              % wheel loaded radius, m
par.m_tire   = 3*4.1;                  % rim mass, kg
par.Ixx_tire = 3*0.12;                   % rim inertia around x-axis, kgm^2
par.Iyy_tire =  3*0.3;                 % rim inertia around y-axis, kgm^2
par.tpf = 'Formula_Student.tir';   % name of the tire property file
tpfarray   = readTPF(par.tpf);      % all parameters from the tire property
                                    % file for Matlab Function

% Road
par.friction = 1;                 % friction coefficient, -
par.rdf = 'TNO_FlatRoad.rdf';       % name of the road data file
rdfarray = readRDF(par.rdf);
% Delft-tyre
use_id = 3114;                      % tire configuration
tyre_mode = [3 1 1 4];
Ttread = 40;                            %Initial Temp
Tcarc = 40;
Tgas = 40;
%%
% load('Skidpad_Spain_2017_bas.mat')
%load('Acceleration.mat')
% load('FSSAutoX1.mat')
load('Endurance.mat')
steer_data = Controller___steeringSteer.Value;
steer_time = Controller___steeringSteer.Time - Controller___steeringSteer.Time(1);

Tfl_data = Controller___Twi__FL_.Value;
Tfl_time = Controller___Twi__FL_.Time - Controller___Twi__FL_.Time(1);

Tfr_data = Controller___Twi__FR_.Value;
Tfr_time = Controller___Twi__FR_.Time - Controller___Twi__FR_.Time(1);

Trl_data = Controller___Twi__RL_.Value;
```

```
Trl_time = Controller___Twi__RL_.Time - Controller___Twi__RL_.Time(1);

Trr_data = Controller___Twi__RR_.Value;
Trr_time = Controller___Twi__RR_.Time - Controller___Twi__RR_.Time(1);

tfl = timeseries(Tfl_data,Tfl_time);
tfr = timeseries(Tfr_data,Tfr_time);
trr = timeseries(Trr_data,Trr_time);
trl = timeseries(Trl_data,Trl_time);
steer = timeseries(steer_data,steer_time);

brake_front_volt = Brake_Pressure_Front.Value/512*5;
brake_front_time = Brake_Pressure_Front.Time-Brake_Pressure_Front.Time(1);
brake_rear_volt = Brake_Pressure_Rear.Value/512*5;
brake_rear_time = Brake_Pressure_Rear.Time-Brake_Pressure_Rear.Time(1);

brake_front = brake_front_volt*260/3.5-(260/3.5*1.5); % Convert voltage to pressure
brake_rear = brake_rear_volt*260/3.5-(260/3.5*1.5);

PistonAmount = 1; %amount of moving piston in one side of the caliper(s) on one wheel
PistonDiameter = .025; %(m) diameter of one moving piston [front,rear]
PistonArea = pi*(PistonDiameter/2)^2; %(m^2) area of one moving piston
PistonAreaTotal = PistonArea*PistonAmount;
DiscRadius = 0.070; %(m) effective brake disc radius
muPad = 0.2; %friction coefficient beTwieen pad and disc

brake_fforce = brake_front*PistonAreaTotal*100000;
brake_rforce = brake_rear*PistonAreaTotal*100000;

brake_ftot = brake_fforce*muPad;
brake_rtot = brake_rforce*muPad;

brake_ftorque = brake_ftot*DiscRadius-3.5;
brake_rtorque = brake_rtot*DiscRadius-4;

Tbf = timeseries(brake_ftorque,brake_front_time);
Tbr = timeseries(brake_rtorque,brake_rear_time);
```

BIBLIOGRAPHY

[1] H.B. Pacejka. *Tyre and Vehicle Dynamics*. Butterworth-Heinemann, 2002.

[2] Formula student germany website.

[3] Formula student team delft website.

[4] M.V. Blundell. The modelling and simulation of vehicle handling part 2: vehicle modelling. *IMechE paper K00399*, 1999.

[5] Yokohama. Aspect ratio.

[6] TNO Automotive. Mf tyre/mf swift 6.2 equation manual, 2013.

[7] Kistler website.

[8] SAE International. Laboratory testing machines and procedures for measuring the steady state force and moment properties of passenger car tires. 1975.

[9] S.B. S.M. David W. Whitcomb, B.A and William F. Milliken. S.b, design implications of a general theory of automobile stability and control. 1956.

[10] Walter Bergman and Claude Beauregard. *Transient Tire Properties*. 1974.

[11] D.L. Milliken W.F. Milliken. *Race Car Vehicle Dynamics*. SAE International, 1995.

[12] Aldo Sorniotti. Tire themal model for enhanced vehicle dynamics simulation. *SAE paper 2009-01-0441*.

[13] D. P. Kelly and R. S. Sharp. Time-optimal control of the race car: influence of a thermodynamic tyre model. *Vehicle System Dynamics, 50:4, 641-662*, 2012.

[14] A.R. Savkoor. Some aspects of friction and wear of tires arising form deformations, slip and stresses at the ground contact. *Wear*, (9(1)), 1996.

[15] K.A. Grosch. The relation between the friction and visco-elastic properties of rubber. *Proceedings of the Royal Society of London*, Series A, Mathematical and Physical Sciences(274(1356)), 1963.

[16] Robert F. Landel Malcolm L. Williams and John D. Ferry. The temperature dependence of relaxation mechanisms in amorphous polymers and other glass-forming liquids. *Journal of the American Chemical Society*, (77(14)), 1955.

[17] P. Fevrier and O. Le Maitre. Tire temperature modelling: Application to race tires. *VDI, Wuerzburg*, 2006.

[18] S. van Rijk. Development and modelling of a formula student racing tyre. *DC 2013.004, Master's Thesis*, 2013.

[19] Abolhasan Nazarinezhad Korbinian Falk and Michael Kaliske. Tire simulations using a slip velocity, pressure and temperature dependent friction law.

[20] Liu W. Eberhardsteiner J. Huemer, T. and H. Mang. A 3d finite element formulation describing the frictional behavior of rubber on ice and concrete surfaces. *Engineering Computations*, (18).

[21] H.B. Pacejka Bakker, E. and L.Lidner. A new tire model with an application in vehicle dynamic studies. *SAE Paper No. 890087*, 1989.

[22] Formula Student Germany. Formula student rules 2017.